COMPLEX PERMITTIVITY MEASUREMENTS DURING HIGH TEMPERATURE RECYCLING OF SPACE SHUTTLE ANTENNA WINDOW AND DIELECTRIC HEAT SHIELD MATERIALS

By Harold L. Bassett and Steve H. Bomar, Jr.

Final Report on

Georgia Tech Project A-1389

Prepared under Contract No. NAS1-11267 by

Engineering Experiment Station
Georgia Institute of Technology
Atlanta, Georgia 30332

for

NATIONAL AERONAUTICS AND SPACE ADMINISTRATION

TABLE OF CONTENTS

LIST OF ILLUSTRATIONS

LIST OF ILLUSTRATIONS (CONTINUED)

LIST OF TABLES

COMPLEX PERMITTIVITY MEASUREMENTS DURING HIGH TEMPERATURE RECYCLING OF SPACE SHUTTLE ANTENNA WINDOW AND DIELECTRIC HEAT SHIELD MATERIALS

By Harold L. Bassett and Steve H. Bomar, Jr.
Engineering Experiment Station
Georgia Institute of Technology

SUMMARY

Thermal and electrical measurements have been performed on six candidate space shuttle antenna window materials: Lockheed LI-1500, McDonnell Mullite HCF, hot pressed boron nitride, Philco-Ford AS-3DX, General Electric Markite 3DQ, and slip-cast fused silica. The material samples were cycled ten times through a simulated reentry surface temperature profile.

During temperature cycling, surface and internal temperatures were measured and the complex microwave transmission coefficient was obtained using a free-space phase shift bridge technique. Using these measured data, the dielectric constant and loss tangent of each material as functions of temperature were calculated to determine whether these properties deteriorated with repeated temperature cycling.

INTRODUCTION

Scope of the Program

The scope of this research program was to perform measurements to determine the values of dielectric constant and loss tangent of several candidate Space Shuttle antenna window and heat shield materials as detailed functions of temperature during exposure to high temperature recycling tests.

Modifications to the high temperature complex permittivity measurement system developed by the Engineering Experiment Station of the Georgia Institute of Technology under two Air Force Contracts (Ref. 1,2) were made so that the complex permittivity of candidate heat shield and antenna window materials could be measured during exposure to Space Shuttle reentry surface temperature profile recycling tests.

Statement of the Problem

The change in electrical properties of electromagnetic window materials as a function of temperature recycling is not known. Since the basic structure of the NASA Space Shuttle will be used on ten or more flights, it was believed necessary to determine the change in electrical properties of candidate electromagnetic window materials as a function of reentry flight time and as a function of temperature recycling. Each candidate material was subjected to a temperature versus time profile designed to simulate the anticipated reentry flight profile. The materials were heated on one side by gas torches and the rate of heating was controlled during the measurement runs to obtain the required surface temperatures on the samples. Each sample was subjected to ten temperature cycles. Two samples of each material type were run. A free-space microwave phase shift bridge was used to measure the change in transmission properties of the materials as a function of time. Dielectric constant and loss tangent data were obtained from the transmission and temperature data.

Background

There has been considerable research in the determination of the electrical properties of materials as functions of temperature. Of particular

interest are the works of Westphal (Ref. 3,4), Bowie (Ref. 5), and Gilreath (Ref. 6). These researchers have used the short circuited waveguide technique (Ref. 7,8) to determine the complex permittivity of materials as a function of temperature. In the short circuited waveguide technique the material of interest is inserted into a metallic sample holder which is enclosed within a furnace. Microwave transmission measurements are then made to determine the complex permittivity. Excellent results are obtained from this technique to temperatures approaching 1923° K (3000° F). The material sample is heated in a near uniform manner so that the whole sample is tested at the particular temperature of interest.

For the recycling measurements it was felt necessary to subject the samples to the anticipated flight thermal environment. This necessarily meant that one surface of the samples would be exposed to the heat source. Then, to obtain useful data, a free-space microwave measurement system was employed in obtaining the microwave transmission properties of the material sample as a function of run time.

MEASUREMENT SYSTEM

The focused beam system allows free-space phase and attenuation measurements to be made on electromagnetic window materials at X-band frequencies to very high temperatures. In fact, measurements have been made to temperatures above 2480° K (4000° F). For this particular program the peak temperature was about 1538° K (2300° F). The complex permittivity versus temperature function is determined from the transmission properties of the material. Past research programs at Georgia Tech have utilized this system at both X-band and K_u-band frequencies (Ref. 1,2).

Description of Free-Space Microwave Sysgem

The complete microwave system is diagrammed in Figure 1. The basic system employs the free space phase-shift bridge and transmission technique described by Redheffer (Ref. 9) to determine the complex permittivities of materials. The focused beam system forms the sample arm of the microwave bridge. The other arm of the bridge is the reference path for the microwave signal. The material specimen is placed in the focal region of the prolate spheroidal focusing reflector normal to the beam axis in the sample arm, and the resulting change in electrical path length is measured by an audio phase detector network. Simultaneously, the attenuation due to the sample is measured. The complex permittivity is computed from these transmission data. Electrical measurements can be performed either in a static or a dynamic thermal environment since the phase and amplitude data are measured and recorded on a continuous basis without having to adjust a mechanical phase shifter.

The technique used to obtain the phase and amplitude data is as follows: A phase-locked CW carrier frequency, f_o, is used both as the frequency of transmission for the focused beam and for the generation of a reference signal, f_o + 1000 Hz. As depicted in Figure 1, the reference signal is mixed with the carrier signal at three single-ended crystal mixers to obtain incident, reflected and transmitted signal measurements. The 1000 Hz mixer outputs are amplified and recorded for amplitude data. Simultaneously, the phase characteristics ϕ_1 and ϕ_2, of the transmitted and incident signals

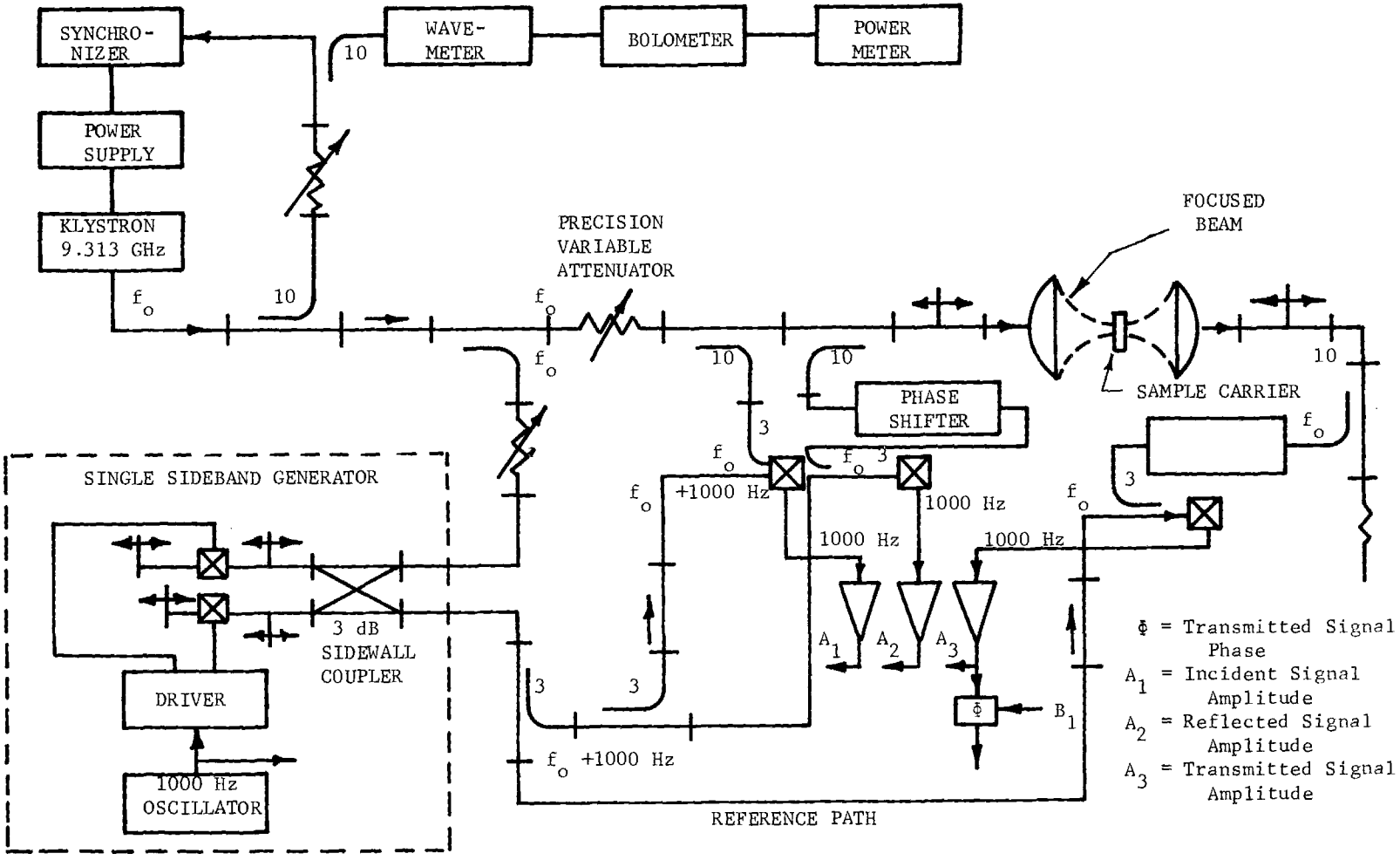

Figure 1. Schematic Diagram of Free-Space Microwave Permittivity Measurement Equipment.

respectively are measured by two phase detectors. The 1000 Hz input reference signal to the phase meters is the same signal that is used to modulate the single-sideband generator network. These phase and amplitude data are recorded on a multichannel recorder.

The single-sideband generator utilizes a 3-dB sidewall hybrid coupler terminated with PIN diodes modulated by a 1000 Hz square-wave signal to generate the f_o + 1000 Hz reference signal. The slide screw tuners, as shown in Figure 1, are adjusted to obtain the proper amplitude and phase relationships of the signal in the two hybrid arms.

The microwave system, as described, can be used to measure the transmission properties of a material at (1) ambient temperature, (2) uniform elevated temperature, and (3) in a transient state (temperature gradient). The latter measurements are made as a function of time and correlated with temperature data to calculate the complex permittivity of the material as a function of temperature. The measurements are made at a frequency of 9.313 GHz.

The focused beam is formed by a 117 cm (46-inch) diameter prolate spheroidal reflector which is illuminated by a feed horn placed at the inner focal point of the reflector. The material sample is positioned at the outer focal point of the reflector which is located 109 cm (43 inches) from the reflector apex. The incident beam is focused to a 3.18 cm (1.25-inch) diameter circle (3 dB points) at the outer focal point. An identical reflector, whose outer focal point is coincident with that of the transmitting reflector, acts as the receiving aperture in the free-space bridge. The sample is mounted on a 51 cm (20.5 inch) diameter carrier disk which is enclosed in a furnace that has open windows on each side through which the microwave beam passes. The disk-shaped sample carrier is mounted so that it is revolved about its center, and the microwave beam is incident on a circular area whose center is displaced from the disk center by 17.1 cm (6-3/4 inches).

Description of Sample Rotating and Heating Apparatus

Samples were mounted in a 51 cm (20.5 inch) diameter carrier disc which rotated inside a furnace enclosure. The rotating carrier and mounted samples were heated by natural gas-air flames using techniques very similar

to those developed on two Air Force programs which preceded this contract (Ref. 1 and 2). The only substantial modifications of earlier experimental techniques involved heating the samples for long periods of time through a predetermined temperature versus time profile. Formerly, emphasis had been placed on achieving the highest possible temperatures without regard to the time the run was in progress.

Design and Construction of Apparatus. The microwave waveguides and reflectors were in a fixed position and could not easily be moved. Thus, the sample rotating and heating device was designed to roll on tracks; movement in two directions was provided. First the entire furnace could be translated parallel to the microwave beam to allow measurement of the average value of transmission coefficient. During measurement runs, the furnace was kept in continuous motion in this direction through a distance of ± 1 centimeter from the center position. The second direction of motion was perpendicular to the microwave beam, for installation of samples, calibration and servicing of the equipment.

Figures 2 and 3 show two views of the sample heating furnace and other parts of the system. The basic frame was constructed in a configuration somewhat like a sawhorse on wheels. The mandrel on which the samples turned was located at the end of a horizontal arm which was pivoted at the top of the sawhorse frame to allow vertical adjustment of the sample position. The front half of the furnace box pivoted upward as shown in Figure 3 to permit sample installation and other servicing operations. An electric motor, mounted near the bottom of the frame, drove the rotating mandrel through a speed-reducing gear box and chain drive. A carrier disc with several mounted samples is installed in the furnace and can be seen in the figures.

On the raised section of the furnace, the cone which defines the microwave beam and the gas torch plumbing are visible. Furnace walls were lined with 2.5 cm (1 inch) thick fused silica foam refractory blocks, and the cone was cast from fused silica and lined on the heated side with silica foam. The torches were made up at Georgia Tech using commercially available cast iron burner heads and rigid copper tubing. The burner heads were water cooled; natural gas and air were supplied from manifolds near their respective control valves, and the gas and air were mixed in the large tubes leading to the burner heads. Supplementary oxygen was injected into the

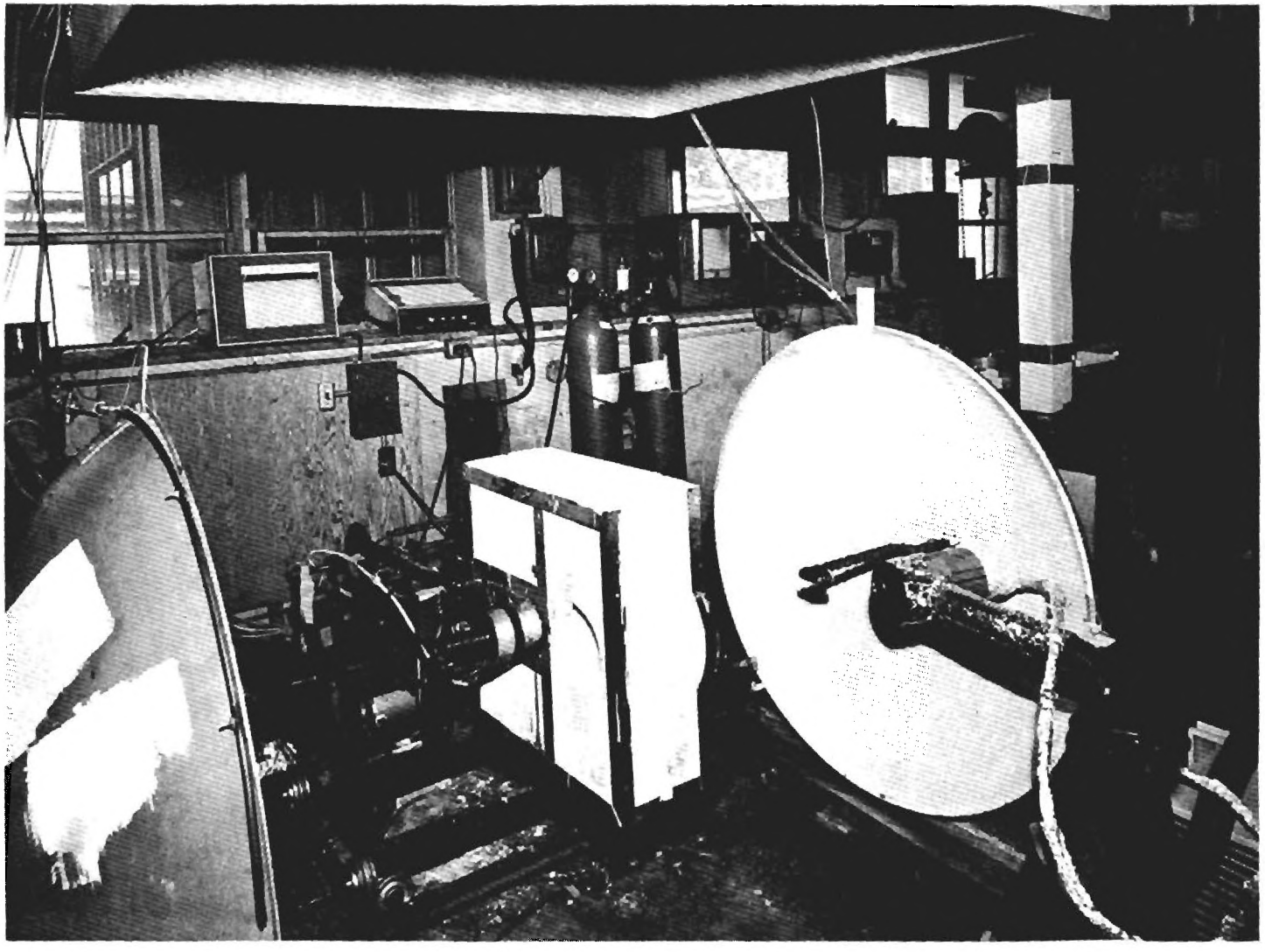

Figure 2. Sample Heating Apparatus, Microwave Reflectors and Optical Pyrometer.

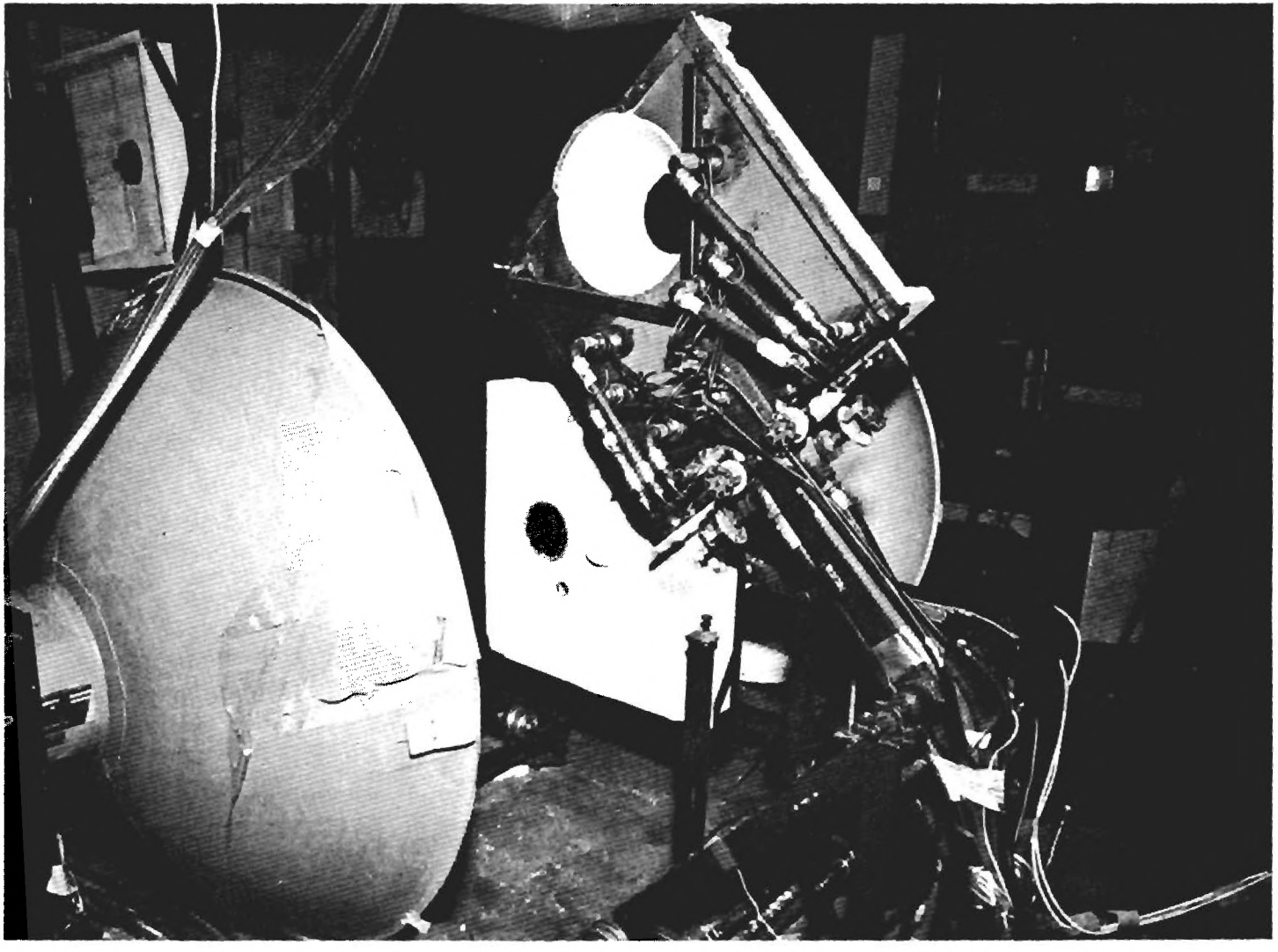

Figure 3. Sample Rotating and Heating Apparatus With Front of Furnace in Raised Position.

combustion air at certain times during the runs to increase combustion temperatures. The six gas torches were located at radii on the carrier which were selected to give uniform heating across the faces of the samples.

The temperature was controlled by manual adjustment of gas, air, and supplementary oxygen flow rates. Time and funds did not permit installation of an automatic temperature control system. The "control temperature" was measured by a thermocouple located on the heated carrier surface. The output of this thermocouple was plotted on an x-y recorder; prior to the run a curve representing the desired front surface temperature versus time was plotted on the recorder chart, so that the furnace operator had a visible record of these temperatures to aid in controlling the furnace.

Samples were centered on a circle at a radius of 17 cm (6.75 in.) from the center of the carrier disc. The furnace was positioned so that the microwave beam passed through the cone, the samples, and the beam hole in the rear furnace wall. When the system was in operation no part of the furnace intruded into the microwave beam. The beam occupies roughly a cone shaped volume in the region near the sample, so that the flame control baffle must be cone shaped.

It was necessary to exercise care to prevent flame attenuation of the microwave beam. In this program, the gas, air, and oxygen flow rates to the torches were adjusted throughout the runs. The ratio of fuel to oxidizing gases was the main factor controlling flame interference; too much fuel gave visible flame in the microwave beam area and significant attenuation could be observed on the microwave recording instruments when this condition existed. Thus, conscious efforts were made to assure that the torches operated with an oxidizing flame. A hood was installed above the sample rotating and heating apparatus for removal of combustion gases from the room, but in contrast to earlier programs this exhaust system played no part in flame control.

The carrier disc was supported on the mandrel assembly shown in Figure 4. The large bearing blocks contained channels for cooling water, and water was continuously circulated through the mandrel assembly. The rotating shaft was provided with 18 small conduits through which thermocouple wires were passed from the rear of the carrier disc to brass slip rings outside the furnace. The slip rings rotated in small troughs filled with mercury to

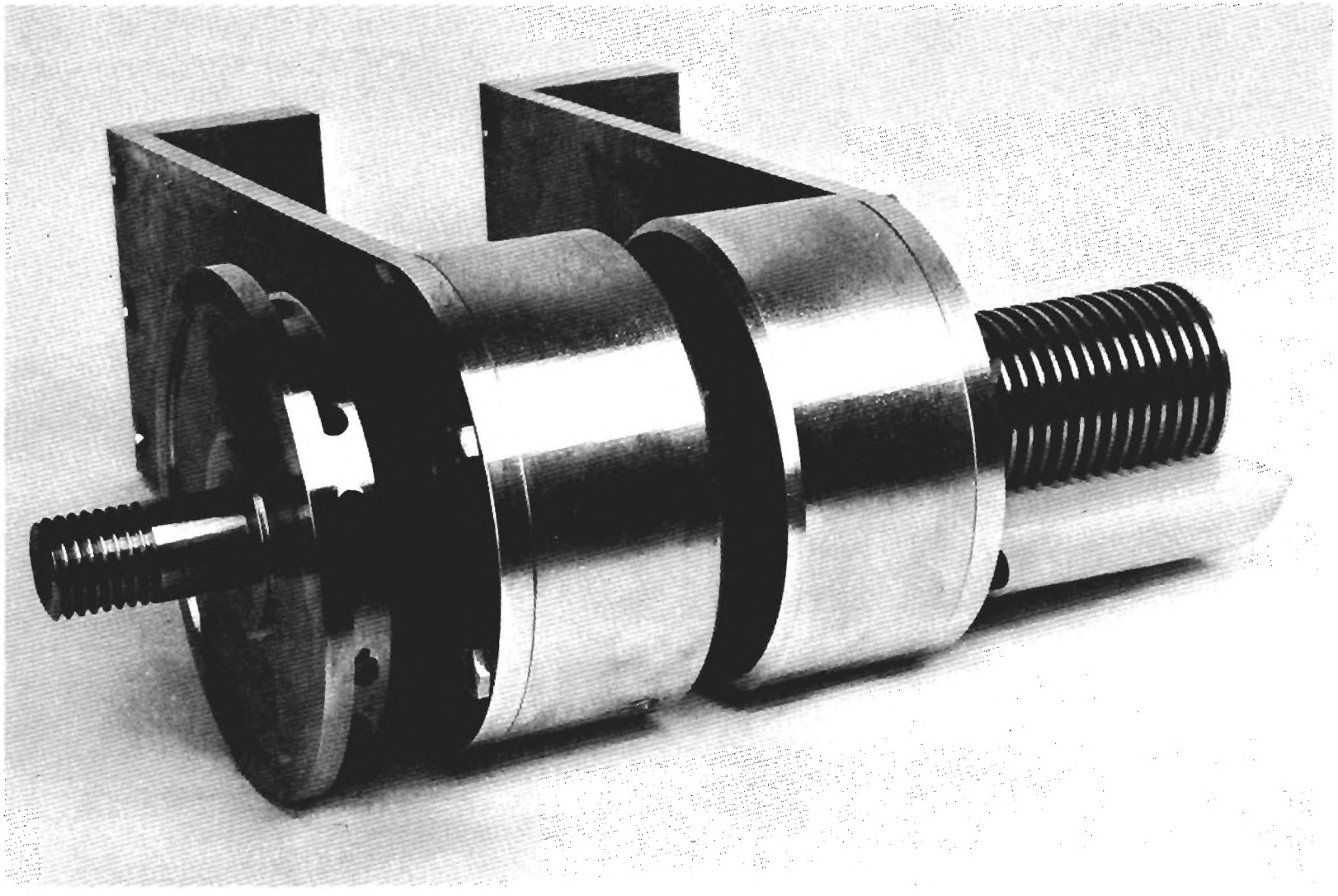

Figure 4. Mandrel Assembly.

conduct thermocouple signals from the mandrel to the recorders.

Two lock nuts were used to retain the carrier disc in place on the end of the mandrel and the nuts were covered by a block of silica foam to protect the threads from damage by flame; also the threaded stud was hollow to permit water cooling. A microswitch and cam were installed on the shaft adjacent to the slip rings to provide an event mark in each revolution; these event marks were placed on all recordings.

Techniques of Surface Temperature Measurement. Optical measurement surface temperatures had been accomplished on an earlier program by the use of fast-response infrared pyrometers. The instruments were Barnes Engineering Company Model IT-4 pyrometers with several custom modifications:

(1) Narrow-band optical filters and unimmersed thermistor bolometers (detectors);
(2) Field of view subtending a 2 cm (0.75-in.) diameter spot at a range of 1.8 m (6 ft.);
(3) Output range from ambient temperature to 2750° K (4500° F) without range switches; and
(4) Electrical output 0 to 5 volts over the temperature range of the instrument with a time constant of 15 milliseconds.

The pyrometers were intended to have sufficiently fast response that the temperatures of individual samples could be measured while the samples were passing by the microwave window. Also, they operated at spectral wavelengths where silica-based materials have high emissivity; passbands of 4.5 μm, 5.1 μm, and 7.9 μm could be obtained with the available filters.

The sensing head of one of these pyrometers is visible in Figure 2, mounted on a stand in front of the right microwave reflector. The pyrometers were sensitive to high ambient temperatures, so that a cooling shield was provided and the shield was cooled by air from a small air-conditioning unit. The field of view was much larger than specified, so that the head required mounting at a short stand-off distance in front of the microwave reflector.

The pyrometer output voltage is directly proportional to target radiance. For a narrow band of wavelengths, target radiance is related to temperature by Planck's law (Ref. 10):

$$N_{b,\lambda} = 2\, C_1 \frac{\lambda^{-5}}{e^{C_2/\lambda T} - 1} \qquad (1)$$

where

$N_{b,\lambda}$ = radiant intensity at λ

C_1 = first constant of Planck's Law = 5.956×10^{-13} watt cm^2

C_2 = second constant of Planck's Law = 1.4387×10^4 $\mu m\ ^\circ K$

λ = wavelength in μm

and T = black body temperature in $^\circ K$.

For a band of wavelengths

$$N_b = \int_{\lambda_1}^{\lambda_2} N_{b,\lambda}\, d\lambda \tag{2}$$

where

N_b = radiance = radiant energy per unit of time,

unit of projected area and unit of solid angle.

This function is not easily integrated between limits λ_1 and λ_2. However, the bandpass interval is very narrow in this case so that we may use the approximation:

$$N_b = N_{b,\lambda}\, \Delta\lambda = \frac{2\, C_1\, \Delta\, \lambda}{\lambda^5 (e^{C_2/\lambda T} - 1)} \tag{3}$$

Barnes Engineering Company furnished a table of radiance vs temperature for each filter and also the cutoff and peak values of wavelength for each filter. Thus sufficient data were available to permit calculation of surface temperatures from the recorded pyrometer output if a calibration could be established. Since the instrument output is a linear function of target radiance, and radiance defines the black-body temperature through Planck's Law, the calibration step must relate output voltage to target radiance. Calibration was performed by measuring the instrument outputs when the pyrometer was pointed at a slip-cast fused silica plate whose temperature was known. The plate was placed behind the door of an electrically heated furnace. The furnace temperature was allowed to equilibrate and the temperature of the target was measured by a thermocouple embedded under

its surface. The pyrometer was pointed at the furnace door and the recorder started. The furnace door was opened quickly for a few seconds to obtain a recording of the pyrometer's response to the hot target. The target temperature began to drop immediately upon opening of the furnace door; thus the pyrometer output at the instant of opening was used for calibration. Calibration data were obtained at several temperatures over the range of interest on this program, and a plot of output voltage vs target radiance was a straight line as expected.

The optical pyrometer recordings were converted to front surface temperatures by a program written for an electronic calculator. The integrated Planck equation (equation 3) can be rearranged to express the temperature as:

$$T = \frac{C_2}{\lambda \ln \left[1 + \frac{2C_1 \Delta\lambda}{\lambda^5 N_b}\right]} \qquad (4)$$

The program was written to input the millimeters of pen deflection read from the recording paper, calculate N_b from the calibration line, calculate the temperature in °K, and print the temperature in °F. A separate program was prepared for each pyrometer, incorporating the appropriate calibration and wavelength constants.

The front surface temperatures reached on this program were low enough to permit the use of front surface thermocouples. Thus, platinum:platinum-13% rhodium couples were installed on the front surface of each thermal sample to check the optical data. It is recognized that metallic thermocouples do not have the same surface characteristics as the ceramic sample materials, and that their temperature responses might not therefore be exactly representative of the samples. However, generally satisfactory agreement between optical and thermocouple temperatures was obtained. Thermocouples have the advantage of better resolution at low temperatures than optical pyrometers.

PREPARATION OF SAMPLES

Six sample materials, candidates for antenna windows in the Space Shuttle thermal protection system, were investigated on this program. Two sets of samples for each material were processed through the test sequence. A set of samples consisted of a nominal 15.2 cm (6-in.) diameter microwave sample and a nominal 3.8 cm (1.5-in.) diameter thermal sample; all thermocouples were mounted in thermal samples because any metal in the microwave samples would interfere with radar measurements.

The preferred sample thickness for these measurements is a multiple of one-half wavelength at room temperature. Adherence to this starting thickness reduces reflections in the microwave system. However, low density materials were run at the thickness as received because trimming would have reduced the quantity of material per unit area and thereby reduced the precision of microwave phase shift and attenuation measurements.

A list of the sample materials and their manufacturers is given in Table I. All samples were supplied to Georgia Tech by NASA-Langley except slip-cast fused silica.

Mounting of Samples

The microwave and thermal samples were mounted in fused silica carrier disks as shown in Figure 5. The carriers were made by pouring a wet casting mixture of fused silica grain and slip into a gypsum plaster mold; the mixture sets as water is drawn into the plaster mold. Holes for the mandrel and samples were formed by locating dense fiberboard plugs of appropriate sizes on the mold before pouring in the casting mixture. After the carrier had set up, the hole plugs were removed and the carrier was dried for several days, then fired at about 1475° K (2200° F) to develop strength.

Chromel-alumel embedded and backside thermocouples and platinum-rhodium front side thermocouples were installed in the thermal samples before samples were mounted in the carriers. Thermocouple leads were made long enough to reach the slip rings after the carrier was mounted on the mandrel. Two embedded thermocouples were positioned along a diameter of the sample, in a 1.2 mm (0.030 in.) wide saw cut at the desired depth. Saw cuts were made from the rear (unheated) side of the sample, and successive cuts were placed

TABLE I

SAMPLE MATERIALS AND MANUFACTURERS

Description	Nomenclature	Manufacturer
Fused quartz reinforced silica composite	AS-3DX	Philco-Ford Corporation
Slip-cast fused silica	SCFS	Georgia Tech
Fiber bundle reinforced silica composite	Markite 3-DQ	General Electric Co.
Silica fiber rigidized coating	LI-1500	Lockheed Missiles and Space Co.
Rigidized mullite fiber	Mullite HCF	Mc-Donnell-Douglas Astronautics Co.
Hot pressed boron nitride	HD-0092	Union Carbide Corporation

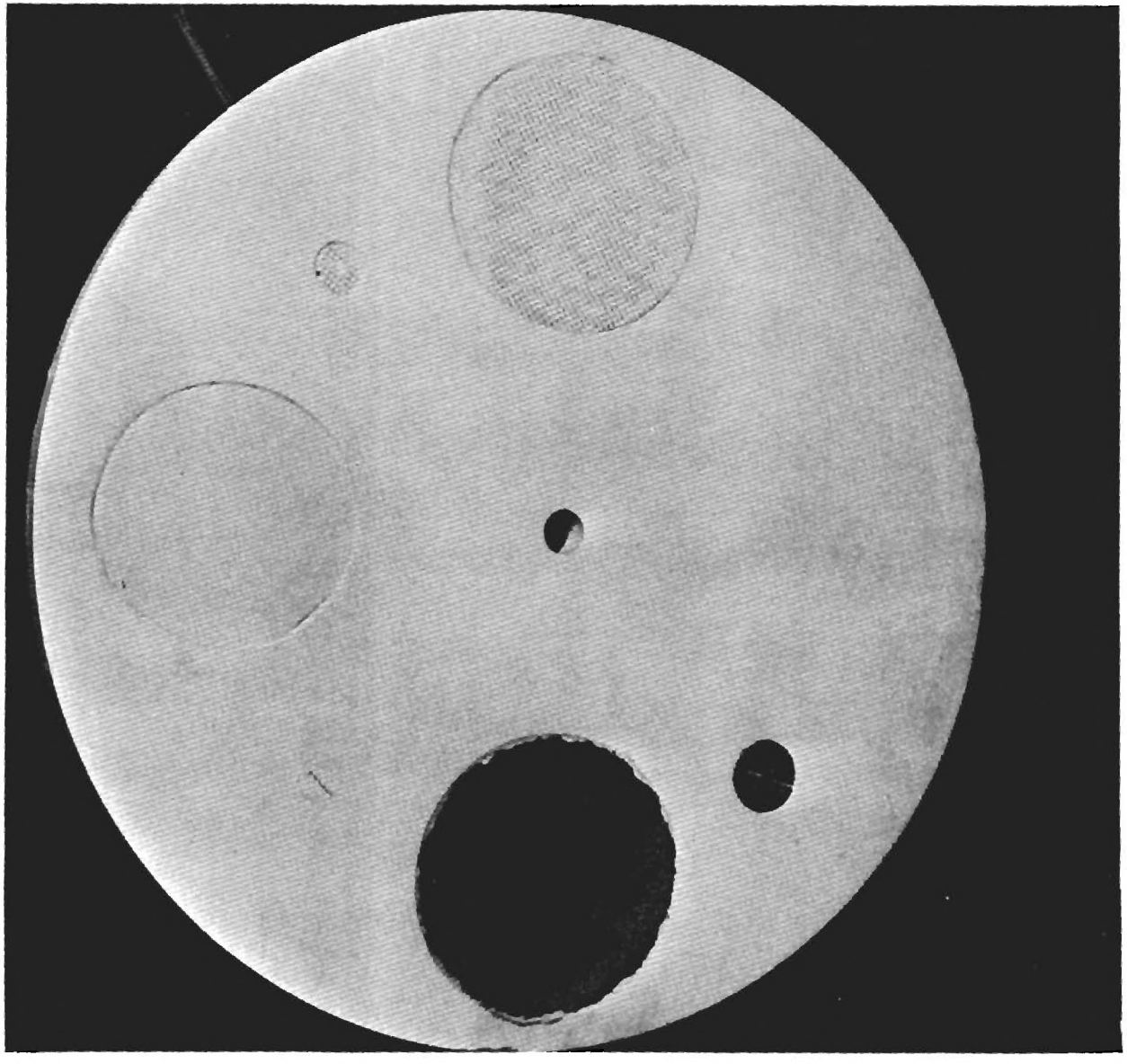

Figure 5. Front View of Carrier Disk and Samples.

on different diameters so that the wires were parallel to the plane of the sample surface but not parallel in other planes. After the wire was positioned in the cut, the cut was filled with a cement made of Ludox AS* (colloidal silica) and powdered sample material. The saw cuts were carefully filled to exclude air bubbles, and the depth of each thermocouple was recorded. After experimental runs, the thermal samples were sectioned to verify thermocouple depths.

The samples were inserted in their respective holes in the carrier disk and anchored by flowing silica cement into the space between the sample and carrier. The samples were positioned with their heated surfaces flush with the front surface of the carrier, as shown in Figure 5. A photograph of the back of this same carrier is shown in Figure 6. Thermocouple wires were covered with silica cement across the back of the carrier to prevent their being damaged by flames during the ten temperature cycles.

Physical Properties of Sample Materials

The physical data given in Table II are for the purpose of documenting the several sample materials. This list is not intended to show all available physical data, but rather to provide data for identifying and characterizing the samples.

Mullite HCF and LI-1500 were run with coatings on the heated surface of the samples. These emittance control coatings were applied by the manufacturers of the two materials, and their compositions and properties were not known to Georgia Tech investigators. In each case, the coatings were less than one millimeter thick.

Carrier and Sample Assignments

Four carriers were run to obtain the required measurements after assembly and check out of the system had been completed. Duplicate specimens of each material were carried ten times through the simulated reentry temperature versus time profile. Samples were assigned to carriers in a manner that precluded running both samples of one material on the same carrier. The materials run on each carrier are shown in Table III.

---

*Trade Mark of E. I. duPont de Nemours and Co.

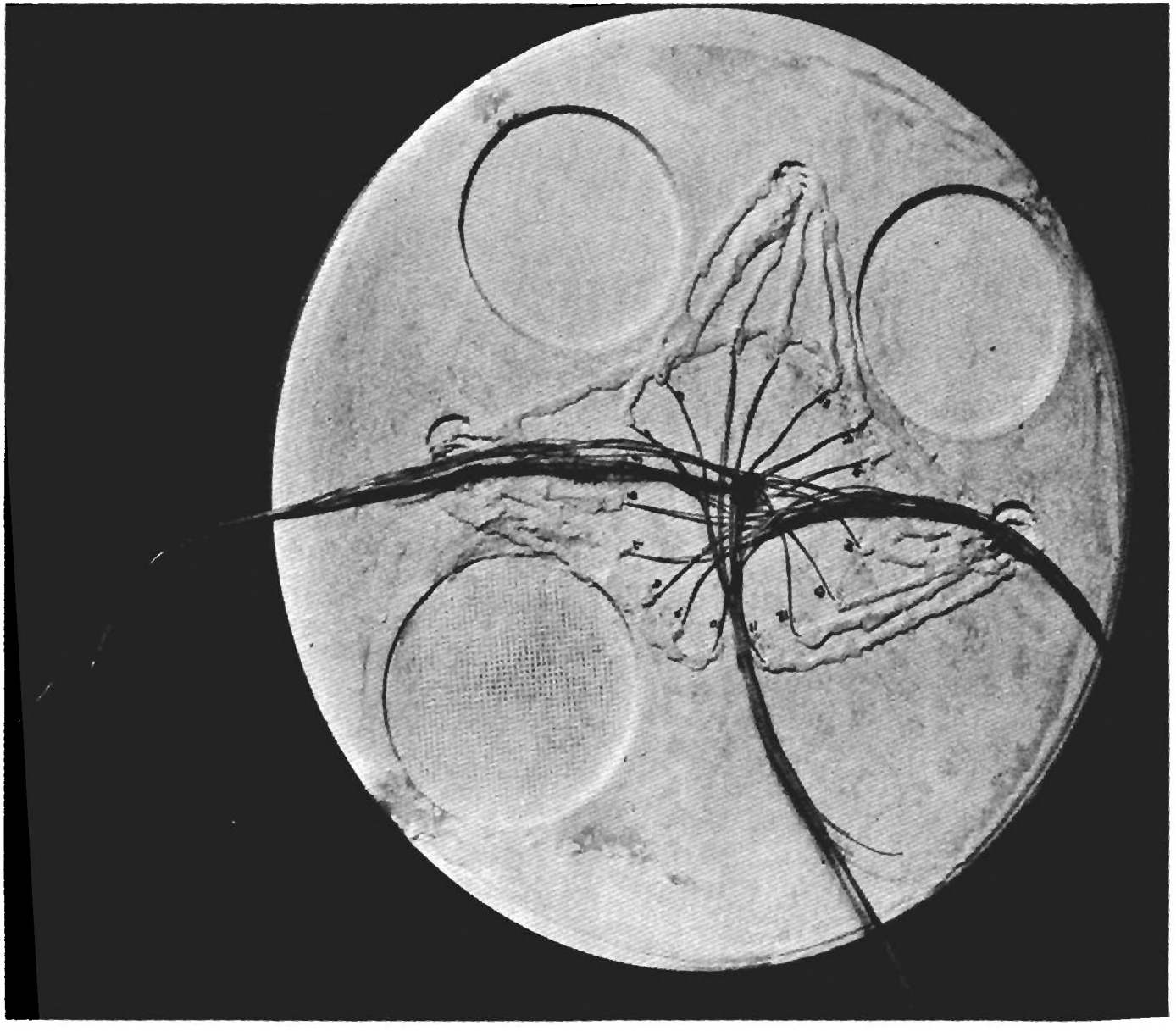

Figure 6. Rear View of Carrier Disk and Samples.

TABLE II

PHYSICAL PROPERTIES OF SAMPLE MATERIALS

Slip-Cast Fused Silica (SCFS)

Slip: Thermo-Materials Corporation, batch 041772-2, high purity
Slip Median Particle Size: 6.9 μm
Firing Conditions: 1478° K (2200° F), 4 hours
Bulk Density: 1.902 gm/cm^3
Silica Content: 99.56 weight per cent

Hot Pressed Boron Nitride (HD-0092)

Boron content: 43.0 to 43.5 per cent
Nitrogen content: 55.6 to 56.3 per cent
Oxygen content: < 1.00 per cent
Carbon content: < 0.4 per cent
Other metallic impurities: 0.05 per cent
Bulk Density: 1.945 gm/cm^3

Fused Quartz Reinforced Silica Composite (AS-3DX)

Bulk Density: 1.673 gm/cm^3

Fiber Bundle Reinforced Silica Composite (Markite 3DQ)

Bulk Density: 1.913 gm/cm^3
Quartz Fibers: 61.47 weight per cent
Silica: 38.53 weight per cent
Porosity: 11.81 volume per cent

Silica Fiber Rigidized Coating (LI-1500)

Bulk Density: 0.237 gm/cm^3 (uncoated)

Rigidized Mullite Fiber (Mullite HCF)

Bulk Density: 0.279 gm/cm^3 (uncoated)
Porosity: 86 volume per cent

TABLE III

CARRIER AND SAMPLE ASSIGNMENTS

Carrier Number	Samples
1	SCFS, Markite 3DQ, Boron Nitride HD-0092
2	AS-3DX, Mullite HCF, LI-1500
3	Boron Nitride HD-0092, AS-3DX, Mullite HCF
4	SCFS, Markite 3DQ, LI-1500

EXPERIMENTAL MEASUREMENT PROCEDURE

The carrier disk containing the mounted samples is installed on the sample rotating and heating apparatus, and thermocouple connections to the recorders are completed. The microwave equipment is allowed to warm up for at least one hour prior to calibration of the system.

To begin calibration, the klystron signal frequency is adjusted to 9.313 GHz and is phased-locked by a synchronizer which maintains a frequency of 9.313 GHz ± 0.0007 MHz. E-H tuners are used to reduce the Voltage Standing Wave Ratio to less than 1.02 at the output and input of the measurement arm, with no furnace or other obstruction in the beam. (It has previously been established that an empty furnace located in the measurement position has no influence on the microwave beam.)

The free-space phase and amplitude calibrations are then made. The incident and transmitted signal calibrations are made by an adjustment of the precision variable attenuator which is shown in Figure 1. The phase calibrations of the transmitted signal are made by adjusting the phase shifter shown in Figure 1. During this operation, signals having known values are placed on the electrical recording charts to assist in subsequent reading of the data.

After the free-space calibration is completed, a static calibration is made on each sample material. The furnace is placed in the measurement position and each microwave sample in turn is rotated into the microwave beam. The variable precision phase shifter is adjusted to determine the room-temperature insertion phase for each sample. The transmission amplitude is determined by moving the sample axially in the beam through a distance of plus or minus one-quarter wavelength and finding the average transmission signal value.

The natural-gas heating torches are lighted to begin the temperature cycle. The output of the control thermocouple is plotted on a recording chart, on which the desired temperature versus time profile has previously been drawn. Gas, air and oxygen flow rates are manually adjusted to follow as closely as possible the specified temperature profile curve.

The following data are recorded versus time: optical temperatures, thermocouple temperatures, change in sample insertion phase, reflection coefficient phase, sample insertion loss, incident power, and reflected power. During the run the sample is continuously moved axially in the microwave beam (± quarter-

wavelength longitudinal displacement) so that the average insertion loss can be determined. The electrical data are recorded on a six-channel visicorder, and the thermal data are recorded on separate recorders. An event mark signal is placed on all recordings once in each carrier revolution so that the response of each sample can be identified. A plot of the target temperature versus time profile is shown in Figure 7.

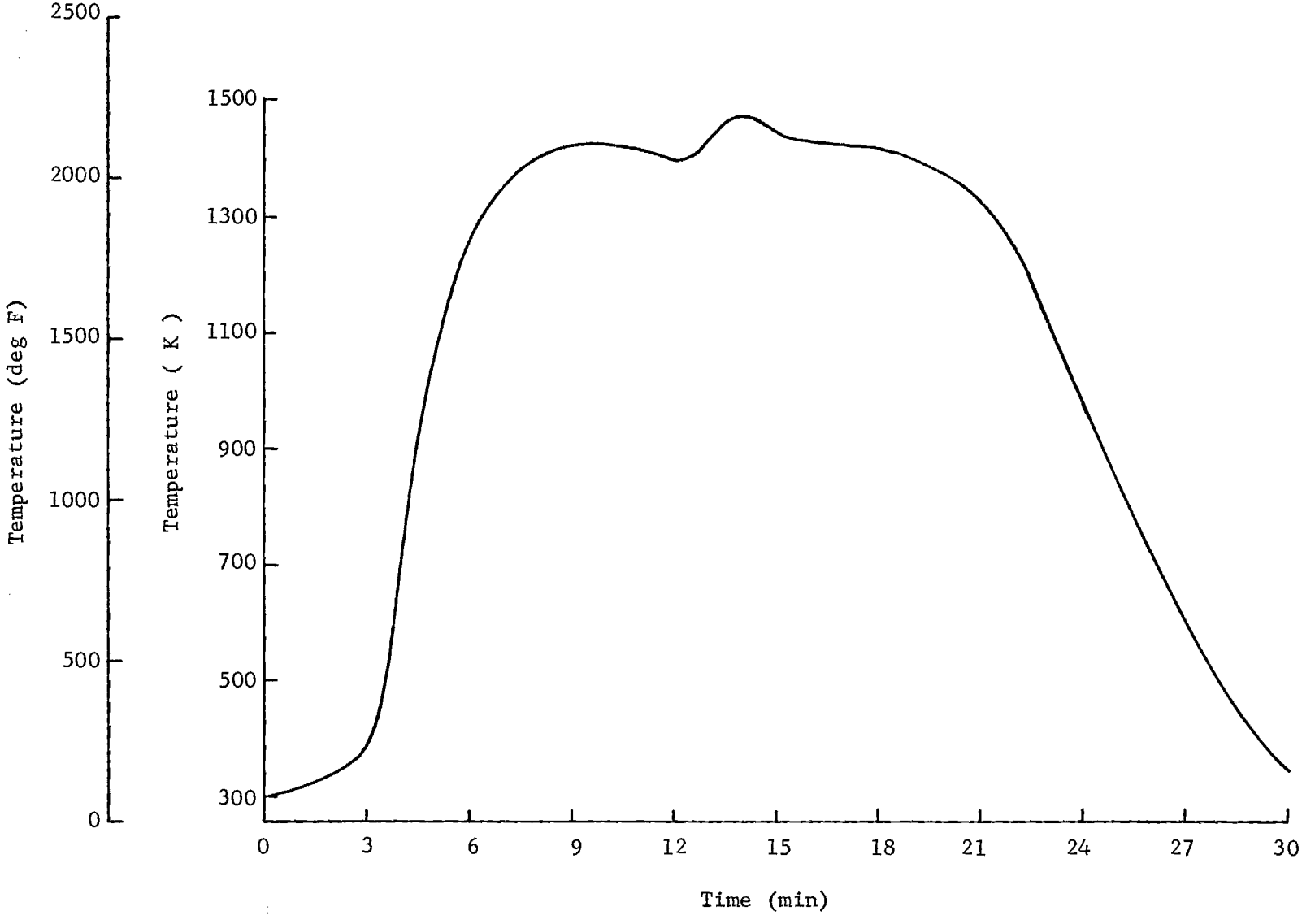

Figure 7. Plot of Target Temperature versus Time.

DATA REDUCTION

The electrical and the thermal analysis programs are written in American Standard Fortran for operation on a UNIVAC 1108 digital computer. This section serves to describe the theories and assumptions involved in the two computer programs.

In order to make the required determinations of dielectric constant and loss tangents as functions of temperature, the electrical analysis program requires temperature profiles and sample thickness as a function of time for each material. The temperature profiles and sample thicknesses are obtained from a thermal analysis program. The temperature profiles and sample thicknesses along with experimentally measured values of the power transmission coefficient and insertion phase delay are used in the electrical analysis computer program to aid in the determination of the piecewise approximations to the relative dielectric constant and loss tangent versus temperature curve for each dielectric material under consideration. This electrical analysis program is essentially the same as the one developed on two earlier Air Force programs (Ref. 1,2). Thermodynamic and transport physical property data with corresponding analytical equations, for all the sample materials are presented in this section. A listing of the thermal analysis program is given in the Appendix; the electrical programs have been published in Reference 2.

Processing of Thermal Data

The thermal analysis program is required to generate temperature versus distance profiles through the sample materials at various times during the experimental run. While the run is in progress, front surface, rear surface, and internal temperatures are recorded. The two surface temperatures and thermal transport properties of the materials are used in the thermal analysis computer program to calculate the required temperature profiles; internal measured temperatures are used to verify that the correct transport properties have been employed and that the program is functioning properly.

Theory. In the measurements performed on this contract, the sample materials never exceeded temperatures on the order of 1530° K (2300° F). Since they were considered candidates for the Space Shuttle thermal protection

system, it was reasonable to expect that no permanent densification or substantial thermal expansion would occur. Thus, the thermal computer program was developed with the following assumptions:

(1) Heat flow was one-dimensional in the axial direction, and
(2) Density was constant and heat capacity and thermal conductivity were functions of temperature.

An energy balance over a thin slab of material whose flat faces are perpendicular to the direction of heat flow gives:

$$\rho V c_p \Delta T_n = \left[k(T_{n+1} - T_n) - k\,(T_n - T_{n-1}) \right] \frac{A\Delta\tau}{\Delta x} \qquad (5)$$

where

ρ = density of the material

c_p = heat capacity

k = thermal conductivity

ΔT_n = temperature in the slab, which we call the nth layer

$\Delta\tau$ = increment of time over which the heat balance is taken

A = area of the slab perpendicular to the direction of heat flow

V = volume of the slab

Δx = thickness of the slab, and

n = a distance index identifying successive slabs.

Simplifying and noting that $V = A\Delta x$, one obtains

$$\rho\, c_p\, \Delta T_n = \frac{k\Delta\tau}{(\Delta x)^2} (T_{n+1} + T_{n-1} - 2T_n) \qquad (6)$$

In this equation, ΔT_n represents the change in temperature of the nth slab, during the time interval $\Delta\tau$. Note that ΔT_n is uniquely expressed in terms of the thermal transport properties (ρ, c_p and k), a time interval ($\Delta\tau$), the slab thickness (Δx) and three temperatures existing at the beginning of the time interval.

Various equations of this type could be written to describe the temperature in a slab, but the one shown was selected because it can be conveniently evaluated using a digital computer. The sample is divided into a number of imaginary slabs, usually 20. The transport properties of each slab are calculated based on its temperature. Then the temperature of each slab is calculated at the new value of time. The program continues to make time steps, calculating a new temperature versus distance profile after each time step. The front and rear surface temperatures are specified by input data.

O'Brien, Hyman and Kaplan (Ref. 11) discuss the stability and convergence of numerical solutions of partial differential equations, and one of their examples is the one-dimensional heat conduction equation with a diffusivity ($k/\rho c_p$) of unity. They concluded that 10 to 20 layers are sufficient to achieve convergence (approach to the true solution), and also observed certain requirements for maintaining stability (damping of errors rather than growth of errors). The stability requirements impose limits on the relative sizes of time increments and slab thicknesses.

Thermal Transport Properties of Samples. As stated earlier, density was assumed constant for all samples in this study; the fact that the temperature cycle was chosen to permit multiple cycling of the materials implied that no permanent change in density would occur. Densities used in the thermal analysis program are given in Table IV.

TABLE IV

DENSITIES OF SAMPLE MATERIALS

Material	Density (gm/cm^3)
SCFS	1.902
AS-3DX	1.673
Markite 3DQ	1.913
HD-0092	1.976
Mullite HCF	0.279
LI-1500	0.237

The heat capacity of solids is a function of temperature and pressure only, provided the material does not experience a phase or structural change. Since all measurements on this program were made at a pressure of one atmosphere, the heat capacities were functions of temperature only. This dependence was represented by an equation of the form

$$c_p = a + bT + c/T^2$$

where

c_p was expressed in units Btu/lb-m $^{\circ}R$

T was expressed in units $^{\circ}R$, and

a, b and c were constants derived from experimental data.

The form of this equation results from considerations of the statistical thermodynamic description of solids; this subject is discussed in many standard thermodynamic texts such as Lewis and Randall (Ref. 12). Experimental heat capacity data were furnished by NASA for LI-1500 and Mullite HCF. These data had been previously collected by Georgia Tech for the other materials (Ref. 2). Values of the heat capacity equation constants are given in Table V.

TABLE V

CONSTANTS FOR THE HEAT CAPACITY EQUATION*

Material	Constants		
	a	b	c
SCFS	0.245	0.142×10^{-4}	-0.250×10^{5}
AS-3DX	0.245	0.142×10^{-4}	-0.250×10^{5}
Markite 3DQ	0.245	0.142×10^{-4}	-0.250×10^{5}
HD-0092	0.339	0.514×10^{-4}	-0.516×10^{5}
Mullite HCF	0.250	0	0
LI-1500	0.300	0.810×10^{-5}	-0.480×10^{5}

*Heat capacity and temperature units are given in the text.

The thermal conductivity of amorphous or glassy materials has been reported by Jakob to be proportional to some power of the temperature (Ref. 13). Jakob also showed that for non-metallic crystalline substances the conductivity is inversely proportional to temperature. Materials investigated on this program included a combination of these types, so that a conductivity equation having this form was selected

$$k = a + b/T + cT + dT^3$$

where

k was expressed in units Btu/hr ft $^{\circ}R$

T was expressed in units $^{\circ}R$, and

a, b, c and d were constants derived from experimental data.

Experimental data were furnished by NASA for LI-1500 and Mullite HCF; they had previously been collected by Georgia Tech for other materials. Manual adjustment of conductivity was required in some cases to obtain satsifactory agreement among internal thermocouple temperatures and temperatures calculated by the thermal analysis computer program. The conductivity was chosen as the property to be adjusted in these cases, because it is generally less well established than density or heat capacity. For example, thermal conductivity is a function of sample density, and density often varies among individual specimens of the same material. Values of the conductivity equation constants are given in Table VI.

TABLE VI

CONSTANTS FOR THE THERMAL CONDUCTIVITY EQUATION*

Material	Constants			
	a	b	c	d
SCFS	0.477	0	-0.183×10^{-4}	0.187×10^{-10}
AS-3DX	0.310	0	-0.119×10^{-4}	0.122×10^{-10}
Markite 3DQ	0.477	0	-0.183×10^{-4}	0.187×10^{-10}
HD-0092	9.060	0.151×10^{4}	0	0
Mullite HCF	0.051	0	-0.167×10^{-4}	0.108×10^{-10}
LI-1500	0.078	-0.207×10^{2}	-0.181×10^{-4}	0.106×10^{-10}

*Thermal conductivity and temperature units are given in the text.

Thermal Analysis Computer Program. The computer program receives input data in the form of front and rear surface temperatures at discrete times during the experimental run. Also, the appropriate thermal property constants are stored for use when needed. The sample is divided into a series of imaginary layers (usually 20) and initial values of variables are established. The first time step is made (typically 0.5 second) and the two surface temperatures at the new instant in time are calculated by linear interpolation of input times and temperatures. Then the temperature of each internal layer is calculated using equation (2) and the first profile is complete. A decision on whether to print the profile is made, another time step is taken, new surface temperatures are calculated, and the next set of internal temperatures is calculated; this completes the second profile. This process continues until the front surface begins final cooling (about 20 minutes after the start of the run), at which time the temperature profiles are not usable for reduction of electrical data. A flowchart of the thermal program is shown in Figure 8.

Processing of Electrical Data

Background. A homogeneous sample of high-temperature dielectric material is heated on one side so that the temperature distribution in the sample is given by $T(x,t)$, where x is the distance from the "cold" side and t is time. The heated sample is positioned in a free-space, focused-beam waveguide bridge. A continuous record in time is made of the temperatures at discrete stations in the sample as well as of the measured values of power transmission coefficient and insertion phase delay of the sample. The duration of the measurements is on the order of 2400 seconds; i.e., the time required for the heated side of the sample to reach maximum temperature and cool to approximately 366° K (200° F). It is desired to find the temperature dependence of the relative dielectric constant and loss tangent of the material from these measurements.

A digital computer program has been prepared to aid in determining the piecewise linear approximations to the relative dielectric constant versus temperature curve and the $\log_{10}$ (loss tangent) versus temperature curve for the material test sample. The program is written in Fortran IV for running on the Univac 1108 computer at Georgia Tech.

Theory. An optimization technique is used to determine the piecewise linear approximations to the ϵ_r vs. T and $\log_{10}$ (tan δ) vs. T curves which

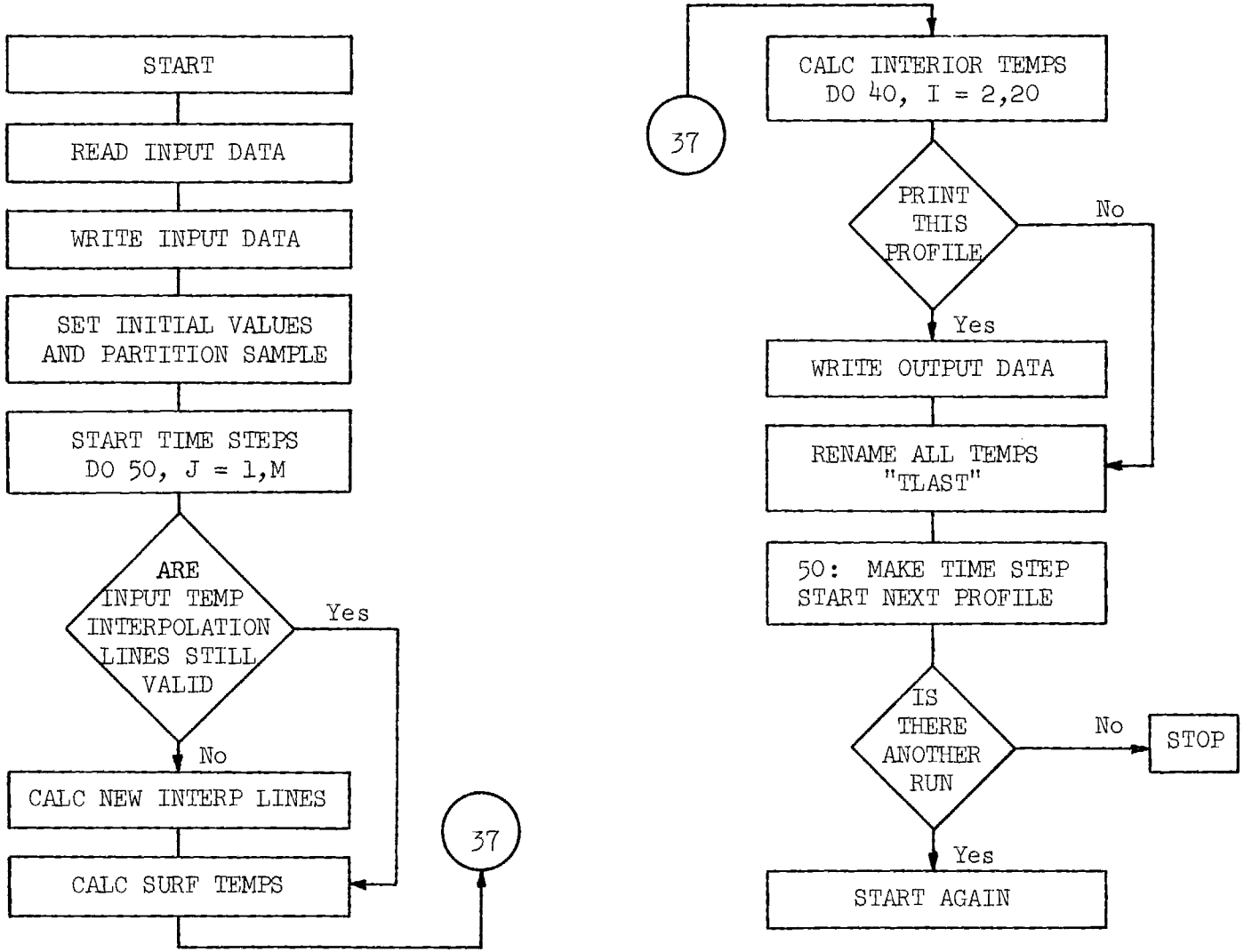

Figure 8. Flow Chart for Thermal Analysis Computer Program.

minimizes the root mean square error between the measured and computed values of power transmission coefficient and insertion phase delay at discrete times, $\underline{t}$: $\{t_1, t_2, \ldots, t_{LL}\}$, in the experimental run. The ϵ_r vs. T curve is specified by the breakpoints of the linear segments comprising the curve. The temperature breakpoints (abscissas) are fixed by physical considerations; the ordinates of the breakpoints are allowed to vary. Thus, the ϵ_r vs. T curve is parameterized using a relatively small number of parameters $\underline{p}$: $\{p_1, p_2, \ldots, p_n\}$. For each sample, we choose n = 5. The $\log_{10}$ (tan δ) vs. T curve is parameterized in a similar manner by the five parameters, $\underline{r}$: $\{r_1, r_2, \ldots, r_n\}$. For each sample, the same temperature breakpoints are chosen for the two curves. These parameters, $\underline{p}$, $\underline{r}$, are adjusted to bring about the optimization.

The temperature at each of M_k stations in the sample at each time, t_K, is computed using the thermal program and the measured temperature data. The "cold" side of the sample is station number 1, the heated surface is station number M_k. The thickness of the sample at each time, t_K, is also determined in the thermal program. These results serve as input data to the present program.

For computation of insertion phase delay, ${}_c\Phi_k$, and power transmission coefficient, ${}_cA_k$, at each time, t_K, the sample is divided into 760 equal-thickness layers. The temperature at the midpoint of each layer is determined by orthogonal polynomial interpolation of the temperatures at the M_k stations in the sample. (Subroutines ORTHLS and FITY.) The relative dielectric constant and loss tangent of each layer are then determined from the current ϵ_r vs. T and $\log_{10}$ (tan δ) vs. T curves. The insertion phase delay and power transmission of the sample at time, t_K, are then computed using the plane dielectric multilayers subroutine, MULTLY.

From the above it is seen that the computed values of transmission coefficient and insertion phase delay are functions of the parameters $\underline{p}$ and $\underline{r}$; i.e.,

$$ {}_cA_k = {}_cA_k\ (\underline{p},\underline{r}) \tag{7} $$

$$ {}_c\Phi_k = {}_c\Phi_k\ (\underline{p},\underline{r}) \tag{8} $$

Experience has shown that the insertion phase delay is a strong function of $\underline{p}$ and has only a relatively weak dependence on $\underline{r}$; also, the transmission coefficient depends more strongly on $\underline{r}$ than on $\underline{p}$. The optimization procedure is thus simplified by representing the computed values of insertion phase delay, ${}_c\underline{\Phi}$, as functions of only $\underline{p}$, and the ${}_c\underline{A}$ as functions of only $\underline{r}$. Since the ϵ_r vs. T curve has the dominant effect in these computations, optimization with respect to this curve is carried out before optimization with respect to the $\log_{10}$ (tan δ) vs. T curve.

The objectives of the computations are to determine the parameters $\underline{p}$ and $\underline{r}$ such that

$$\left[\frac{1}{LL}\sum_{K=1}^{LL}\left[{}_mA_k - {}_cA_k(\hat{\underline{r}})\right]^2\right]^{1/2} \leq {}^{\delta}A \qquad (9)$$

$$\left[\frac{1}{LL}\sum_{K=1}^{LL}\left[{}_m\Phi_k - {}_c\Phi_k(\hat{\underline{p}})\right]^2\right]^{1/2} \leq {}^{\delta}\Phi \qquad (10)$$

where

LL = number of discrete times, t_K

${}_mA_k$ = measured power transmission coefficient at t_K

${}_m\Phi_k$ = measured insertion phase delay at t_K

${}^{\delta}A$ = specified error tolerance in transmission coefficient

${}^{\delta}\Phi$ = specified error tolerance in insertion phase delay

The error tolerances are based on measurement error. For the present version of the program, $\delta_A = 0.004$ and $\delta_\Phi = 1.0$ degree.

The parameters $\hat{\underline{p}}$ and $\hat{\underline{r}}$ which meet the requirements of (9) and (10) are determined in the following way. Initial estimates of the ϵ_r vs. T and $\log_{10}$ (tan δ) vs. T curves are specified in terms of $\underline{p}$ and $\underline{r}$, and ${}_c\underline{A}$ and ${}_c\underline{\Phi}$ are computed for these sets of parameters. The corrections $\underline{\Delta p}$: $\{\Delta p_1, \Delta p_2, \ldots, \Delta p_n\}$ such that

$$\hat{\underline{p}} \triangleq \begin{bmatrix} \hat{p}_1 \\ \hat{p}_2 \\ \vdots \\ \hat{p}_n \end{bmatrix} = \begin{bmatrix} p_1 + \Delta p_1 \\ p_2 + \Delta p_2 \\ \vdots \\ p_n + \Delta p_n \end{bmatrix} \triangleq \underline{p} + \underline{\Delta p} \tag{11}$$

are found using the following scheme. At a given time, t_K, the differential of ${}_c\Phi_k(\underline{p})$ is, by definition,

$$d_c\Phi_k \triangleq \frac{\partial_c\Phi_k}{\partial p_1} \Delta p_1 + \ldots + \frac{\partial_c\Phi_k}{\partial p_n} \Delta p_n \tag{12}$$

The actual change in ${}_c\Phi_k(\underline{p})$ for increments $\underline{\Delta p}$ is

$$\Delta_c\Phi_k = {}_c\Phi_k(\underline{p} + \underline{\Delta p}) - {}_c\Phi_k(\underline{p}) \tag{13}$$

For small $\underline{\Delta p}$, we can equate (12) and (13) to yield

$$\Delta_c\Phi_k = \frac{\partial_c\Phi_k}{\partial p_1} \Delta p_1 + \ldots + \frac{\partial_c\Phi_k}{\partial p_n} \Delta p_n \tag{14}$$

Let ${}_c\Phi_k(\underline{p} + \underline{\Delta p}) = {}_m\Phi_k$ so that

$$\Delta\Phi_k = {}_m\Phi_k - {}_c\Phi_k(\underline{p}) \tag{15}$$

Doing this for each time t_K results in the following matrix formulation:

$$\begin{bmatrix} \Delta\Phi_1 \\ \Delta\Phi_2 \\ \vdots \\ \Delta\Phi_{LL} \end{bmatrix} = \begin{bmatrix} \frac{\partial\Phi_1}{\partial p_1} & \cdots & \frac{\partial\Phi_1}{\partial p_n} \\ \vdots & & \vdots \\ \frac{\partial\Phi_{LL}}{\partial p_1} & & \frac{\partial\Phi_{LL}}{\partial p_n} \end{bmatrix} \begin{bmatrix} \Delta p_1 \\ \Delta p_2 \\ \\ \Delta p_n \end{bmatrix} \tag{16}$$

or

$$\underline{\Delta\Phi} = \underline{J}\ \underline{\Delta p} \tag{17}$$

The approximate partial derivatives are obtained numerically. The elements of the approximate Jacobian matrix, $\underline{J}$, are given by

$$J_{ij} = \frac{{}_c\Phi_i(p_1, p_2, \ldots, p_j + \delta p, \ldots, p_n) - {}_c\Phi_i(\underline{p})}{\delta p} \tag{18}$$

where δp is a small perturbation of p_j. Provided $LL \geq n$, equation (17) can be solved for $\underline{\Delta p}$; i.e.,

$$\underline{\Delta p} = \underline{J}^{-1}\ \underline{\Delta\Phi} \tag{19}$$

where $\underline{J}^{-1}$ is the inverse of the approximate Jacobian matrix $\underline{J}$. If $LL > n$, the system of equations is over-determined and the generalized unique inverse of the non-square matrix, $\underline{J}$, must be used rather than the conventional inverse. Subroutine GID accomplished this.

Having obtained $\underline{\Delta p}$ and, hence, $\hat{\underline{p}}$, the left side of equation (10) is computed and compared to the specified error tolerance, δ_Φ. In general, ${}_c\Phi_k(\hat{\underline{p}})$ will not be equal to ${}_m\Phi_k$ for all $k = 1, 2, \ldots, LL$. Hence, the process would be repeated by finding a new set of corrections to $\hat{\underline{p}}$ found above. However, it is considered advantageous at this point to next apply the optimization procedure to the $\log_{10}$ (tan δ) vs. T curve utilizing the $\underline{r}$ parameters and a duplication of the procedure outlined above for the $\underline{p}$ parameters. In the actual computer program this is done; i.e., the $\underline{p}$ parameters are optimized first, then the $\underline{r}$, then the $\underline{p}$, etc., until equations (9) and (10) are satisfied.

The incremental corrections, $\underline{\Delta p}$, given by equation (19) would ideally be of the order of δp since equation (14) and succeeding equations are valid only for small $\underline{\Delta p}$. In addition, it is possible that equation (19) would yield values of Δp_i which would alter the ϵ_r vs. T curve to the point of being outside physical bounds. Thus, in implementing this scheme on the computer, tests are provided to insure that the $\underline{\Delta p}$ are within physical bounds. In addition, a "fine adjustment" may be applied to the $\underline{\Delta p}$ which consists of multiplying the $\underline{\Delta p}$ by a scalar constant, c, and adjusting this constant until

$$\hat{\underline{p}} = \underline{p} + c\underline{\Delta p} \tag{20}$$

yields a minimum RMS error in the insertion phase delay. Note that as c approaches zero, the corrected ϵ_r vs. T curve approaches the original curve. It was found during the course of the electrical data processing that no fine adjustment was required, resulting in a considerable savings in computational time.

Computer Program. The computer program consists of a MAIN program and the following subroutines: FORWAR, MULTLY, GID, ORTHLS, FITY. The functions of these routines and the variable explanations are adequately described by the accompanying flow diagrams (Figures 9 and 10) and comment cards in the programs. Only a brief description of each of these programs is given below.

MAIN is the calling program and carries out the optimization procedure described previously. FORWAR is called by MAIN to compute the power transmission coefficients, $_c\underline{A}$, and insertion phase delays, $_c\underline{\Phi}$, at the times, $\underline{t}$, for given sets of parameters $\underline{p}$ and $\underline{r}$. FORWAR accomplishes this by dividing the sample into NL = 760 layers, computing the temperature, relative dielectric constant, and loss tangent of each layer using ORTHLS and FITY, and computing $_c\underline{A}$ and $_c\underline{\Phi}$ of the resulting plane multilayer dielectric using MULTLY. MAIN builds the approximate Jacobian matrix, $\underline{J}$, and utilizes GID to find the transpose of the generalized unique inverse of $\underline{J}$. MAIN transposes $[\underline{J}^{-1}]^T$ to give $\underline{J}^{-1}$, solves equation (19), and continues the optimization procedure until equations (9) and (10) are satisfied, or until other externally set conditions are met.

The electrical program has been tested in the following way. A "true" ϵ_r vs. T curve and a "true" $\log_{10}$ (tan δ) vs. T curve were assumed. These curves are piecewise linear curves specified by their abscissa and ordinate breakpoints. Typical input temperature and thickness data obtained from previous work were used as input test data. Using the "true" curves, the values of $_c\underline{\Phi}$, $_c\underline{A}$ were computed. These computed values were then defined as the "measured" data $_m\underline{\Phi}$, $_m\underline{A}$. These values of $_m\underline{\Phi}$, $_m\underline{A}$ were then used as the measured input data. Rather gross estimates of the ϵ_r and tan δ curves were then assumed. These estimates consisted of linear continuations of the known low-temperature 255 to 1644° K (0 to 2500° F), data into the high-temperature regions. The abscissa breakpoints on these estimated curves were the same as for the "true" curves. Using the same input temperature and thickness data as before, the program was allowed to run. The results show that only

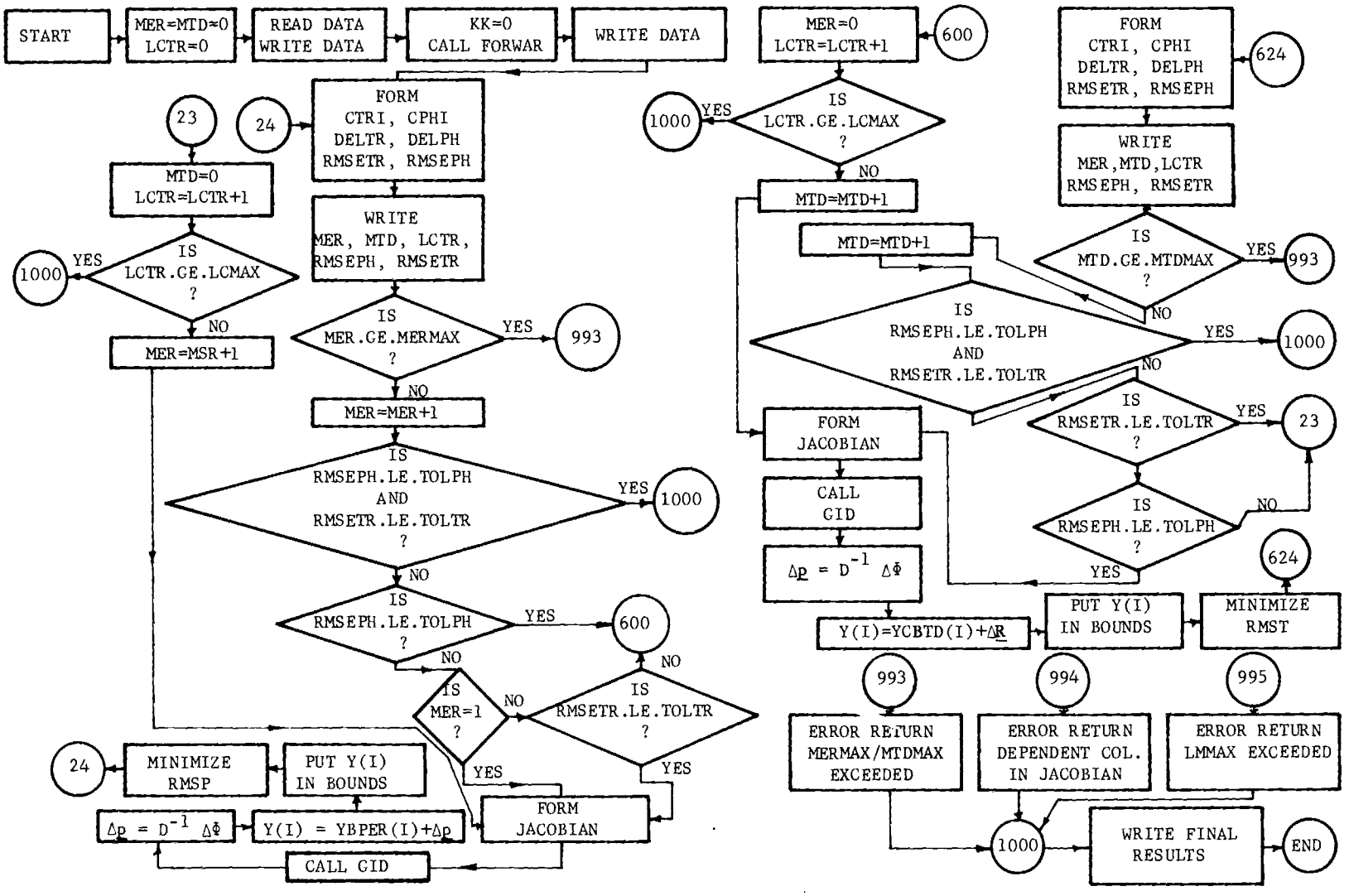

Figure 9. Flow Chart for Electrical Analysis Computer Program.

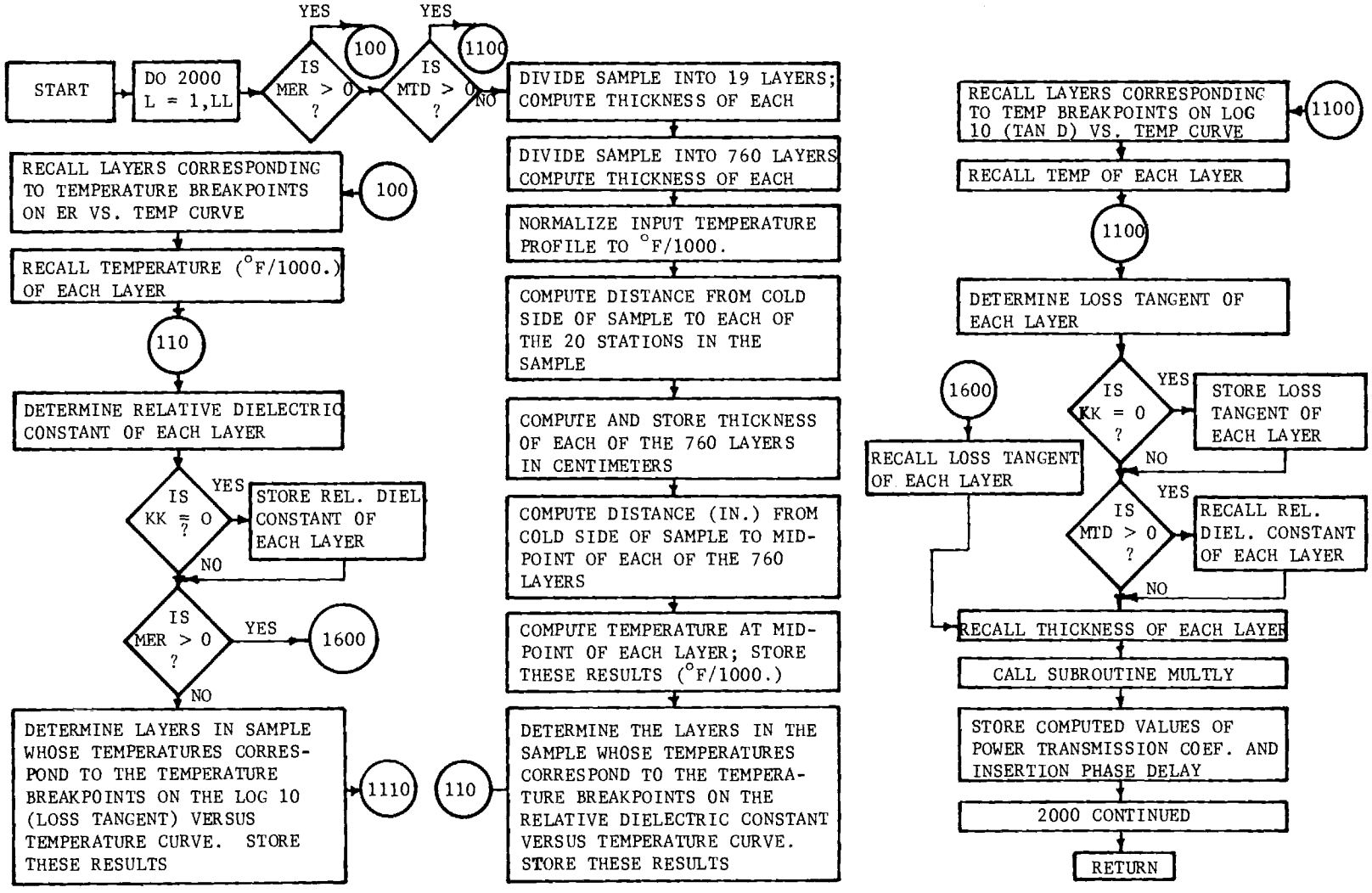

Figure 10. Flow Chart for Subroutine Forwar.

one correction is required on each curve to satisfy equations (9) and (10) when $\delta_{\Phi} = 1.0$ degree and $\delta_{A} = 0.004$. Setting these tolerances to zero and allowing the program to make one more correction to each curve resulted in a corrected curve essentially equal to the "true" curve.

Processed Data. The measured data are surface and internal sample temperatures, insertion phase shift and transmission loss, and incident and reflected power. These are measured as functions of time for each temperature cycle. The thermal data are then processed and the temperature profiles are obtained for each sample as a function of time and cycle number.

The electrical data for each sample are plotted for each temperature cycle. Any deviations in electrical data from run to run are noted. The only significant changes occurred with hot-pressed boron nitride and the AS-3DX composite materials. Boron nitride lost material from the heated surface which amounted to approximately 1.6 electrical degrees in phase change per temperature cycle. The thickness of the boron nitride changed from 1.59 cm (0.627 inches) to 1.52 cm (0.600 inches) during the 10 temperature cycles or 0.0068 cm (0.0027 inches) per cycle. The AS-3DX composite material insertion phase delay at room temperature was affected mostly by the initial temperature runs. The insertion phase delay decreased by 2 degrees after two runs were completed. The room temperature insertion phase delay then remained constant throughout the remainder of the test runs.

The other materials (LI-1500, Mullite, Markite, and slip-cast fused silica) reacted in like manners. During the exposure to the heat, each material had phase shift and transmission loss responses that would be repeated from run to run.

Typical data are plotted in Figures 11 through 16. These data indicate the transmission loss and insertion phase shift averaged over a number of runs. The run time indicated on each diagram can be correlated to temperature by the use of Figures 17 through 22, in which are shown the time-temperature history of the front surfaces of the samples.

The remaining electrical data are presented as dielectric constant and loss tangent values as functions of sample temperature. As explained in the section on Processing of Electrical Data, the dielectric constant and loss tangent are obtained in the following manner. From the measurement run, sample temperature profiles are obtained at eight time intervals. The sample model

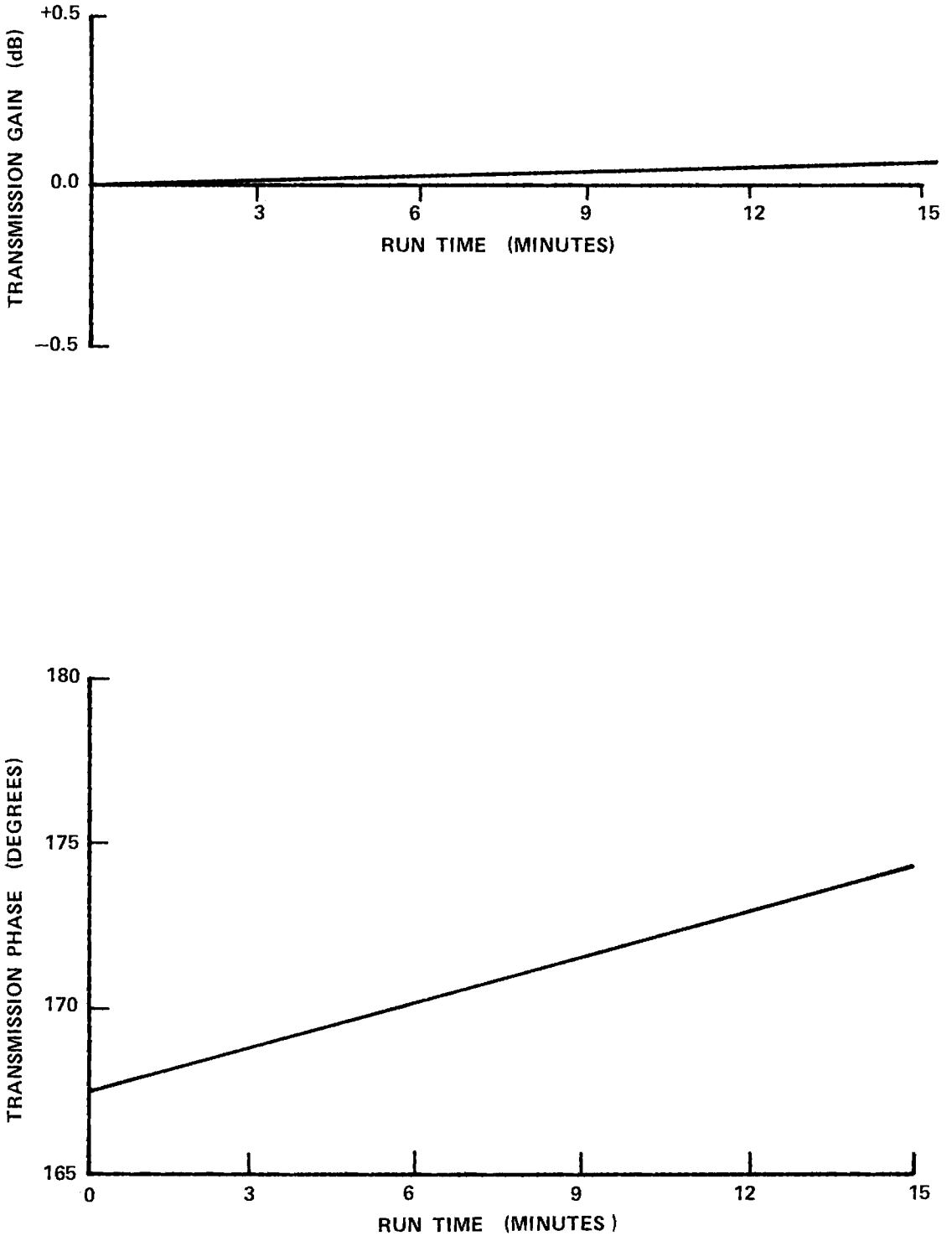

Figure 11. Georgia Tech SCFS: Carrier 1 and 4 Transmission Properties.

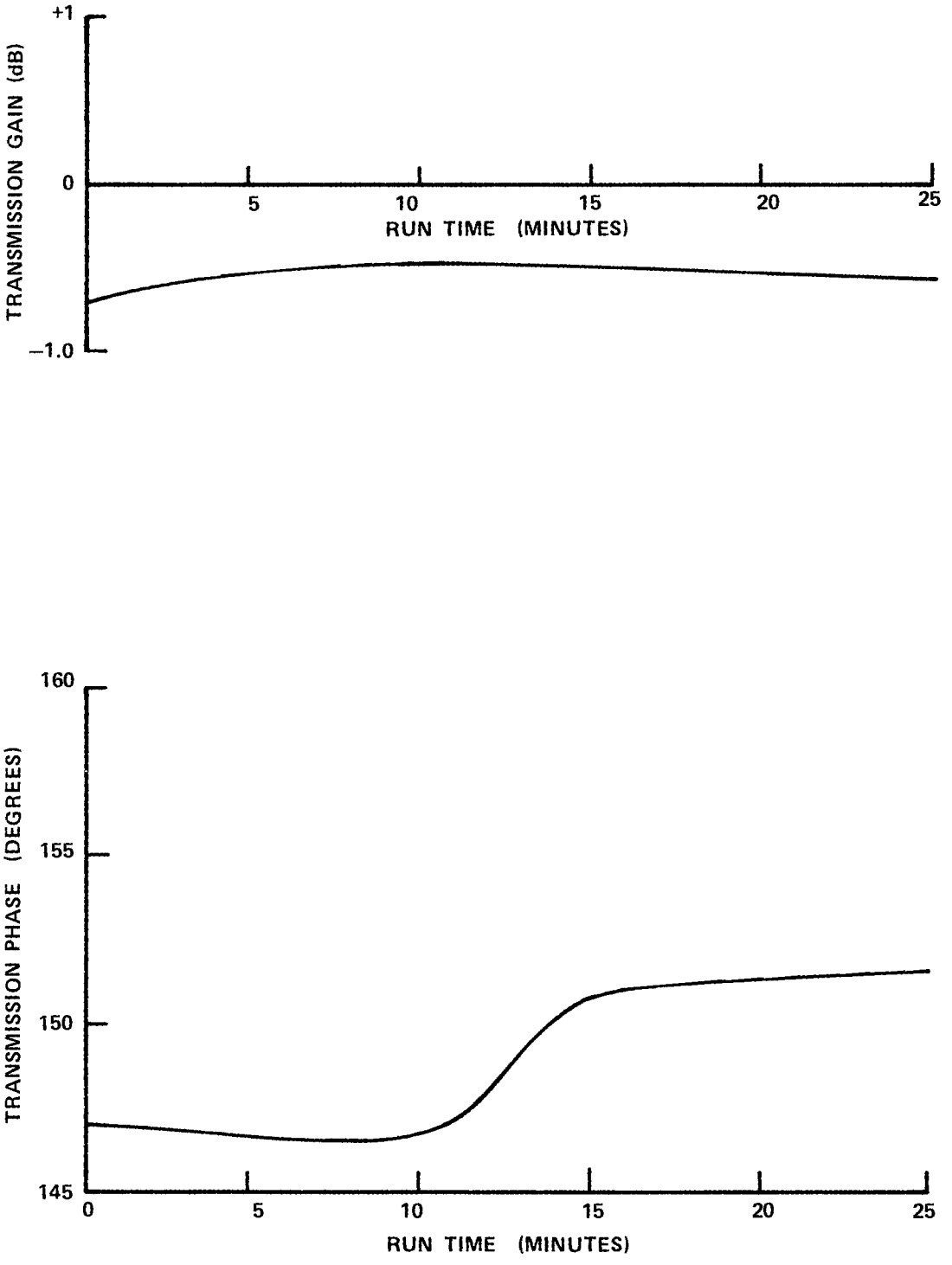

Figure 12. Philco-Ford AS-3DX: Carrier 2 Transmission Properties.

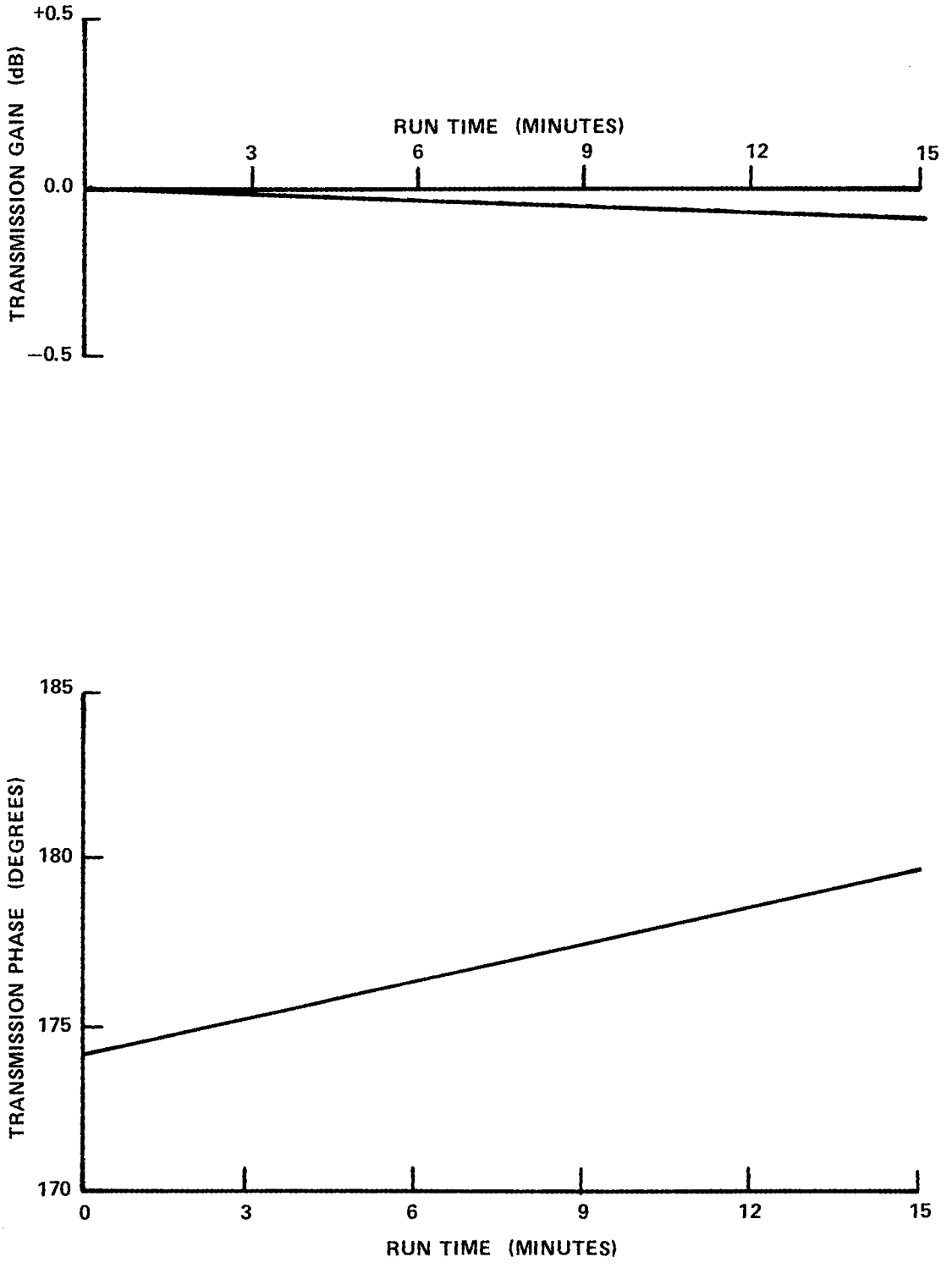

Figure 13. General Electric Markite 3DQ: Carriers 1 and 4 Transmission Properties.

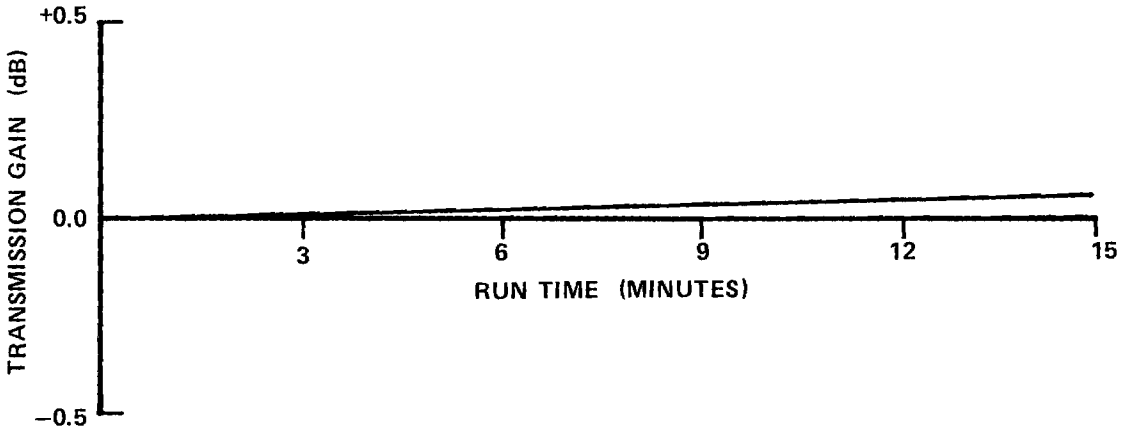

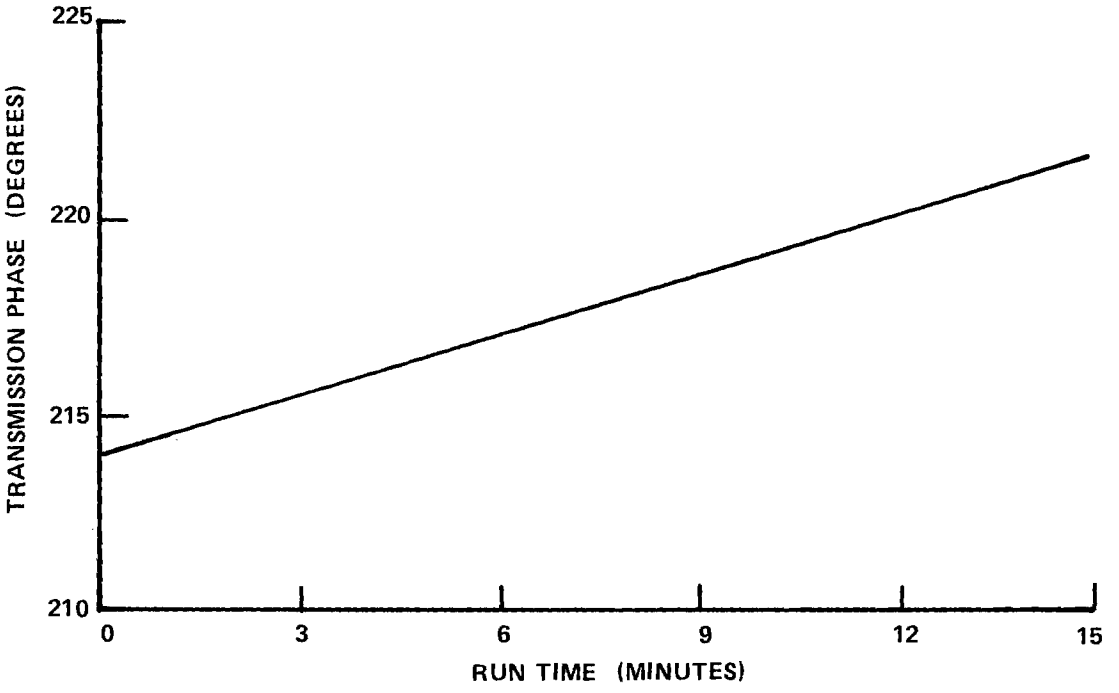

Figure 14. Boron Nitride HD-0092: Carriers 1 and 3 Transmission Properties.

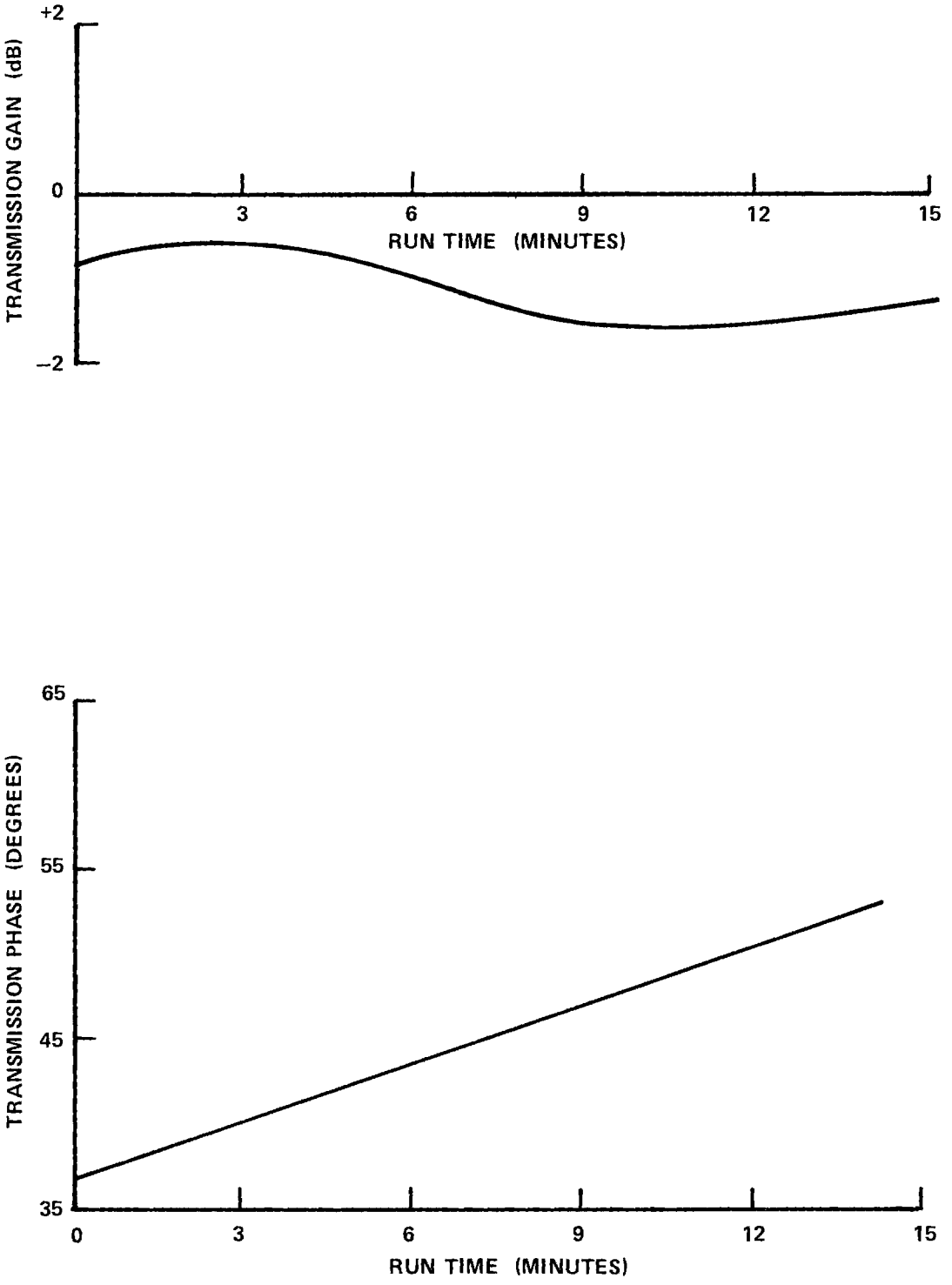

Figure 15. McDonnell Mullite HCF: Carriers 2 and 3 Transmission Properties.

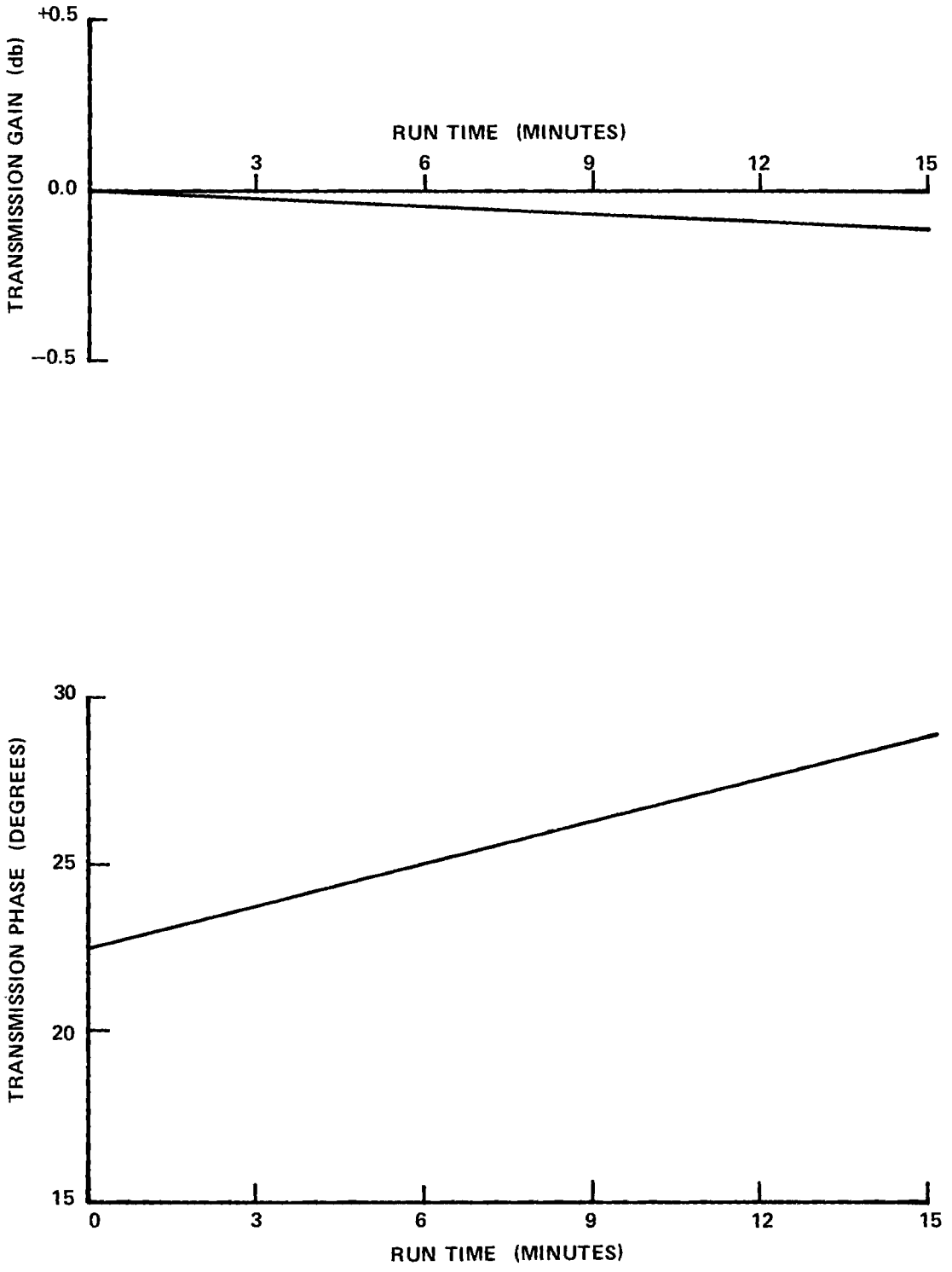

Figure 16. Lockheed LI-1500: Carriers 2 and 4 Transmission Properties.

is divided into 760 layers for each time interval. Assumed dielectric constant and loss tangent values as functions of temperature for the sample are used and each layer is assigned specific values of ϵ_r and tan δ. The multi-layer analysis transmission computer program is then used as a tool to calculate the insertion phase shift and transmission coefficient for these conditions. These calculated data are then compared to the measured insertion phase shift and transmission loss. An error term is generated which is used to perturb the assumed dielectric constant and loss tangent versus temperature curves. Iterations are made until the calculated data approach the measured data. In this manner, the end results are curves of dielectric constant and loss tangent versus temperature for each measured sample. The short-circuit waveguide data obtained from NASA Langley are used as a baseline in the determination of the initial temperature functions. The computed values of dielectric constant and loss tangent are presented in the section entitled Results and Discussion.

RESULTS AND DISCUSSION

Four carrier disks were run for collection of experimental data. Each carrier was exposed to the specified reentry temperature profile ten times, using the temperature of the slip cast fused silica surface for control purposes. (When a carrier contained no SCFS sample, the carrier surface temperature was used for control.) Carrier and sample assignments are given earlier in Table III.

The purpose of this program was to determine whether a deterioration of dielectric properties occurred in the candidate window materials during repeated recycling through a simulated reentry temperature versus time profile. During a typical experimental run, data were recorded for about 18 minutes; there were a total of 40 experimental runs, each involving three sample materials. In view of the magnitude of the data reduction task, it was decided to begin by processing only the first and tenth runs of each carrier. If no deterioration of dielectric properties occurred between the first and tenth runs, then no further information would be gained by processing the intermediate runs. If deterioration was observed, then intermediate runs could be processed as required. Runs 1, 5 and 10 of the first carrier were evaluated, and Runs 1 and 10 of subsequent carriers were completely processed.

Thermal Data

Figures 17 through 22 show typical temperature versus time profiles for each of the sample materials. The three silica based materials (SCFS, AS-3DX and Markite 3DQ) all showed the same temperature response behavior to the heating environment. We were unable to reach the rate of rise desired at the beginning of the runs, but successfully matched the desired maximum temperatures. We believe that the temperature exposure was a reasonable simulation of the desired reentry profile, however. Note also that the difference between front and back surface temperatures was on the order of 200° K (400° F) throughout the runs for these materials.

The boron nitride (HD-0092) samples experienced a somewhat slower rate of front surface temperature rise than did the silicas, but they also reached the desired maximum temperature. The difference between front and rear surface temperatures was on the order of 100° K (200° F). The lower rate of rise and

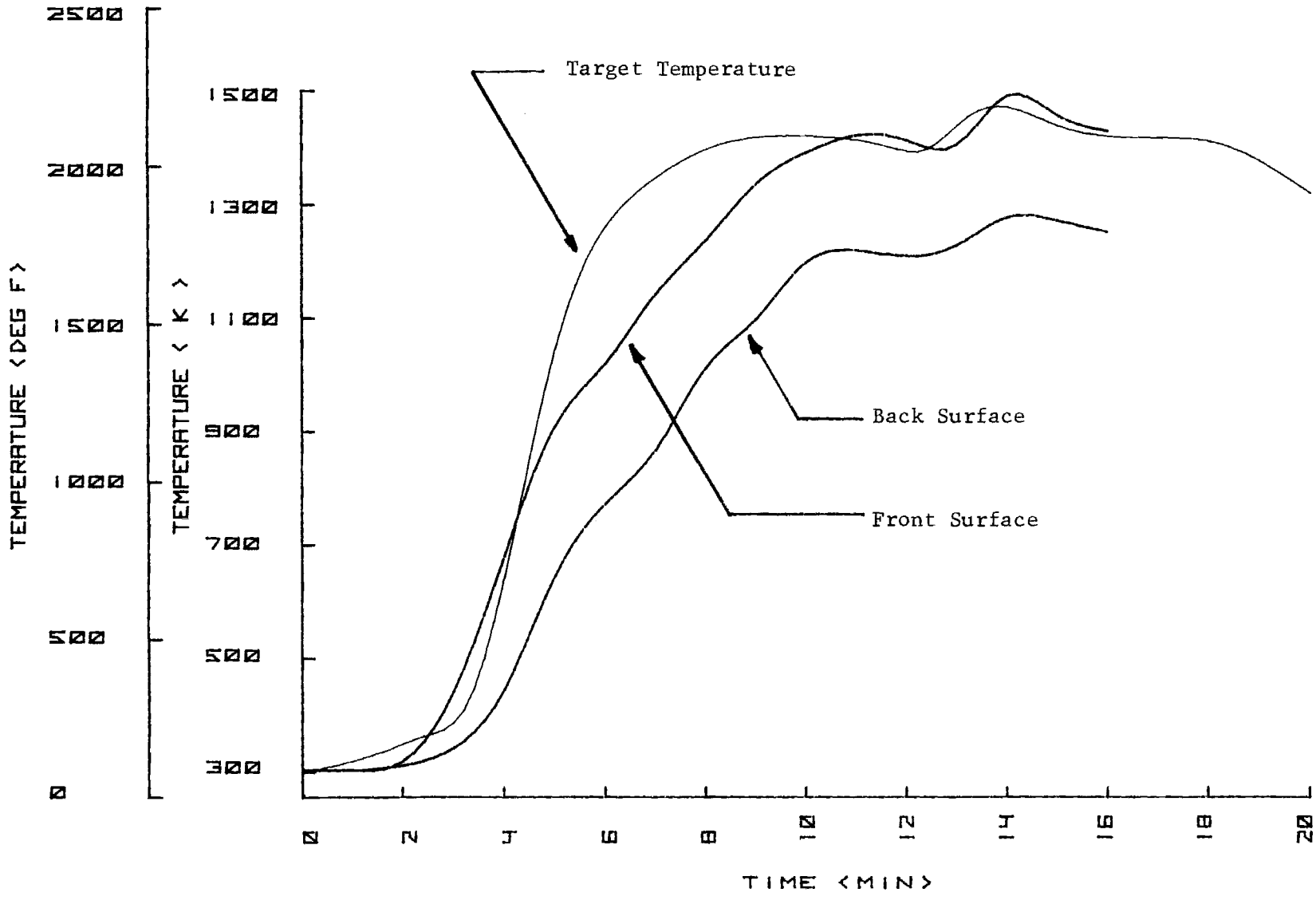

Figure 17. Typical Temperature versus Time Plot for Slip-Cast Fused Silica.

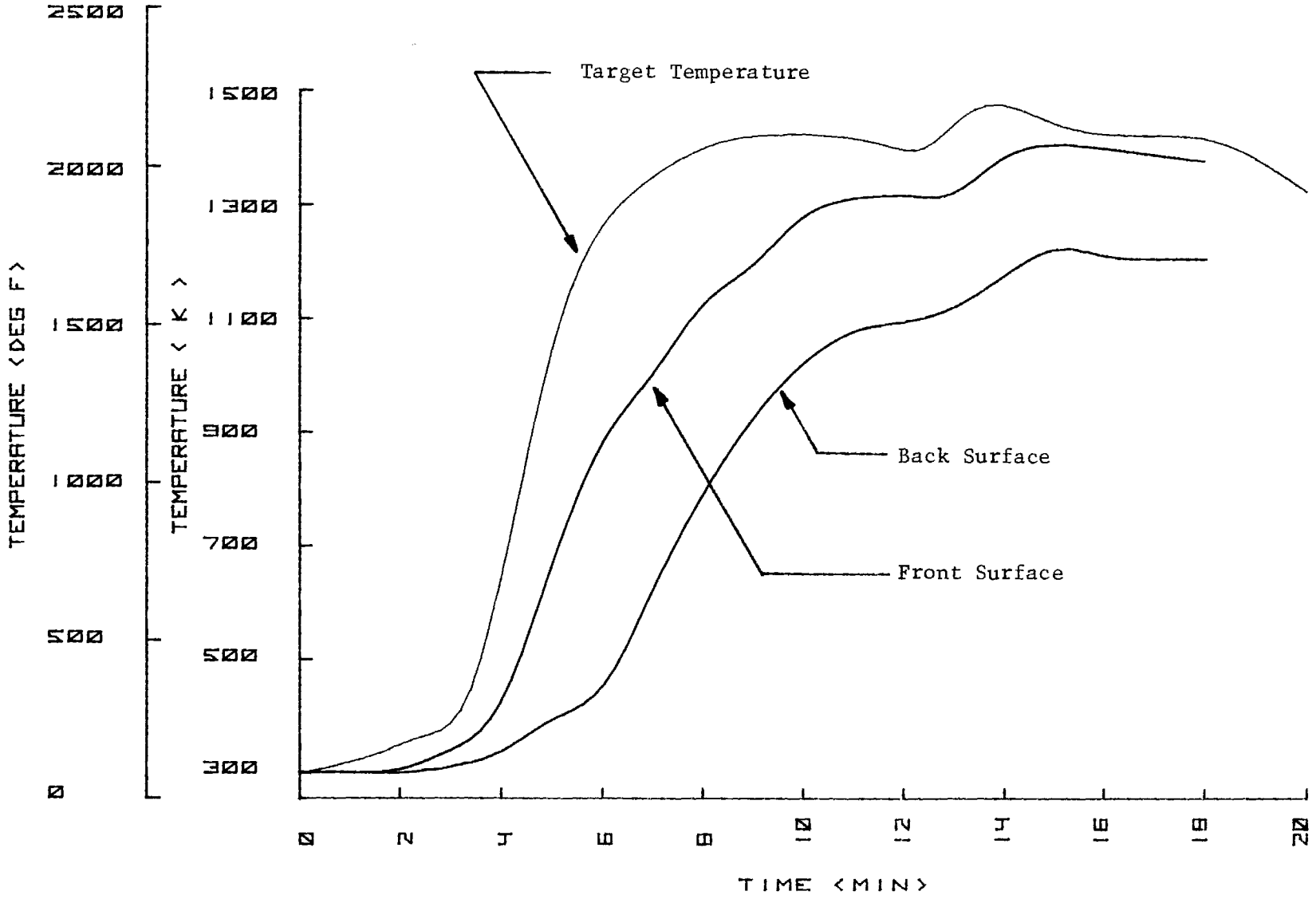

Figure 18. Typical Temperature versus Time Plot for AS-3DX.

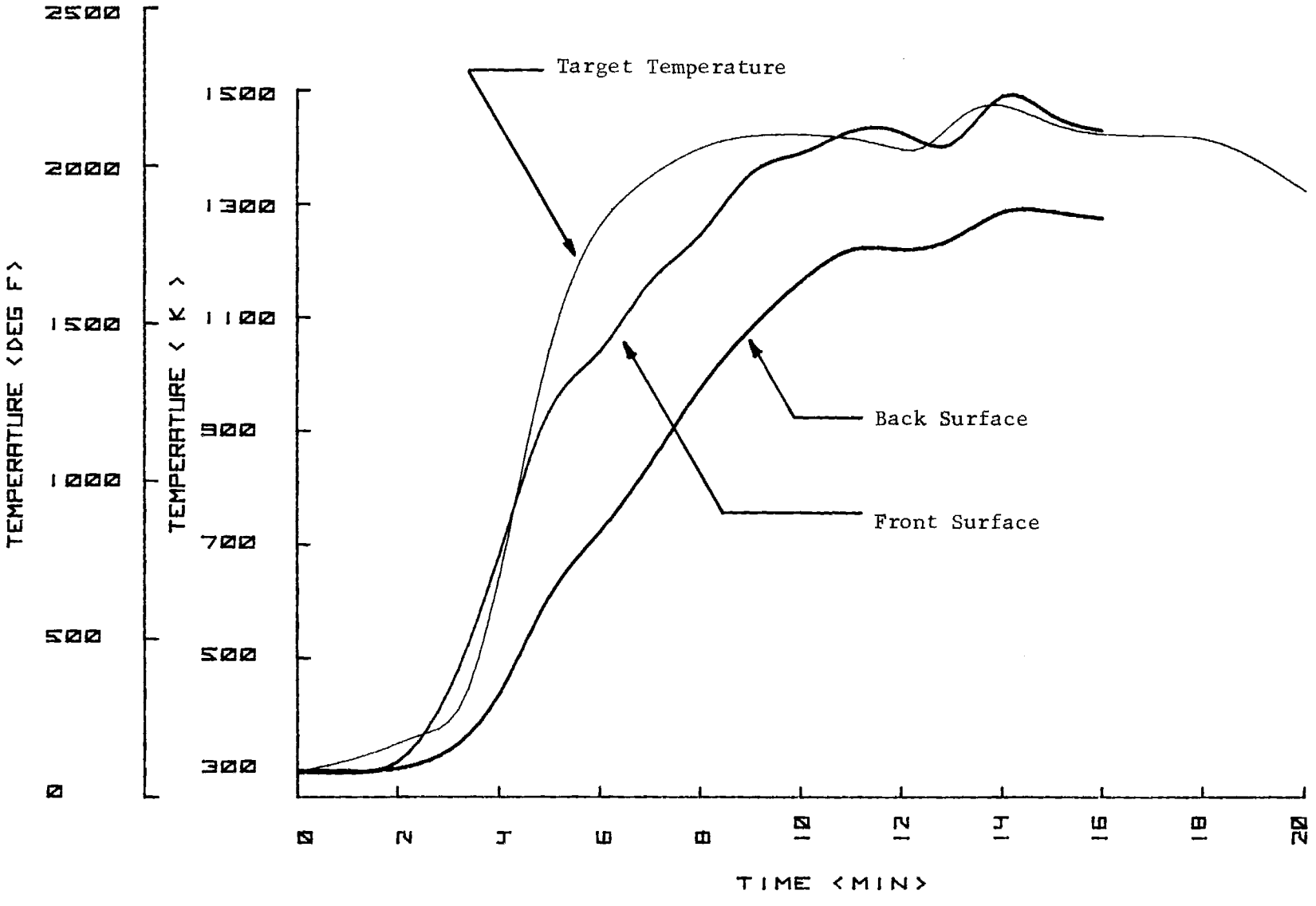

Figure 19. Typical Temperature versus Time Plot for Markite 3DQ.

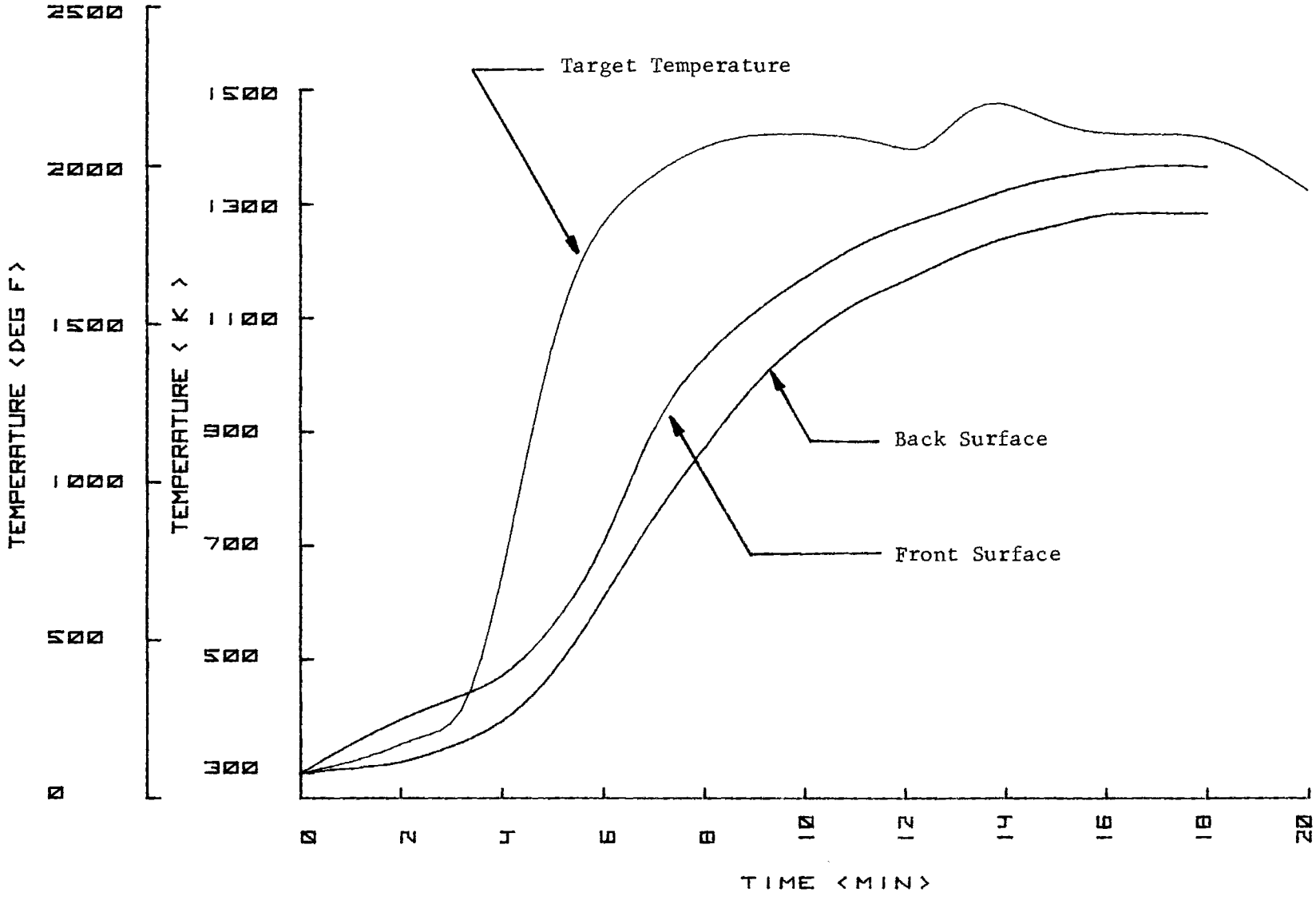

Figure 20. Typical Temperature versus Time Plot for Boron Nitride (HD-0092).

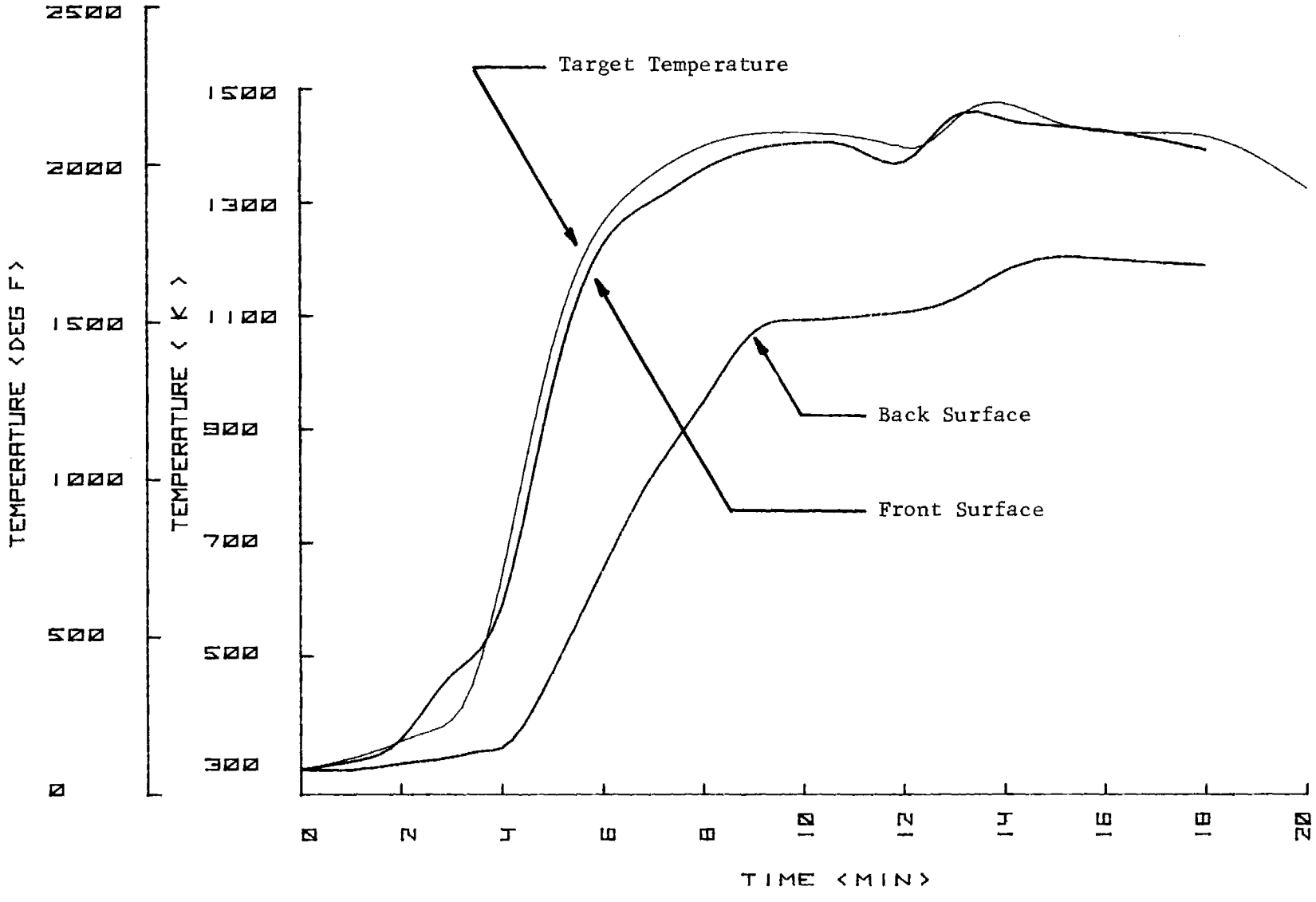

Figure 21. Typical Temperature versus Time Plot for Mullite HCF.

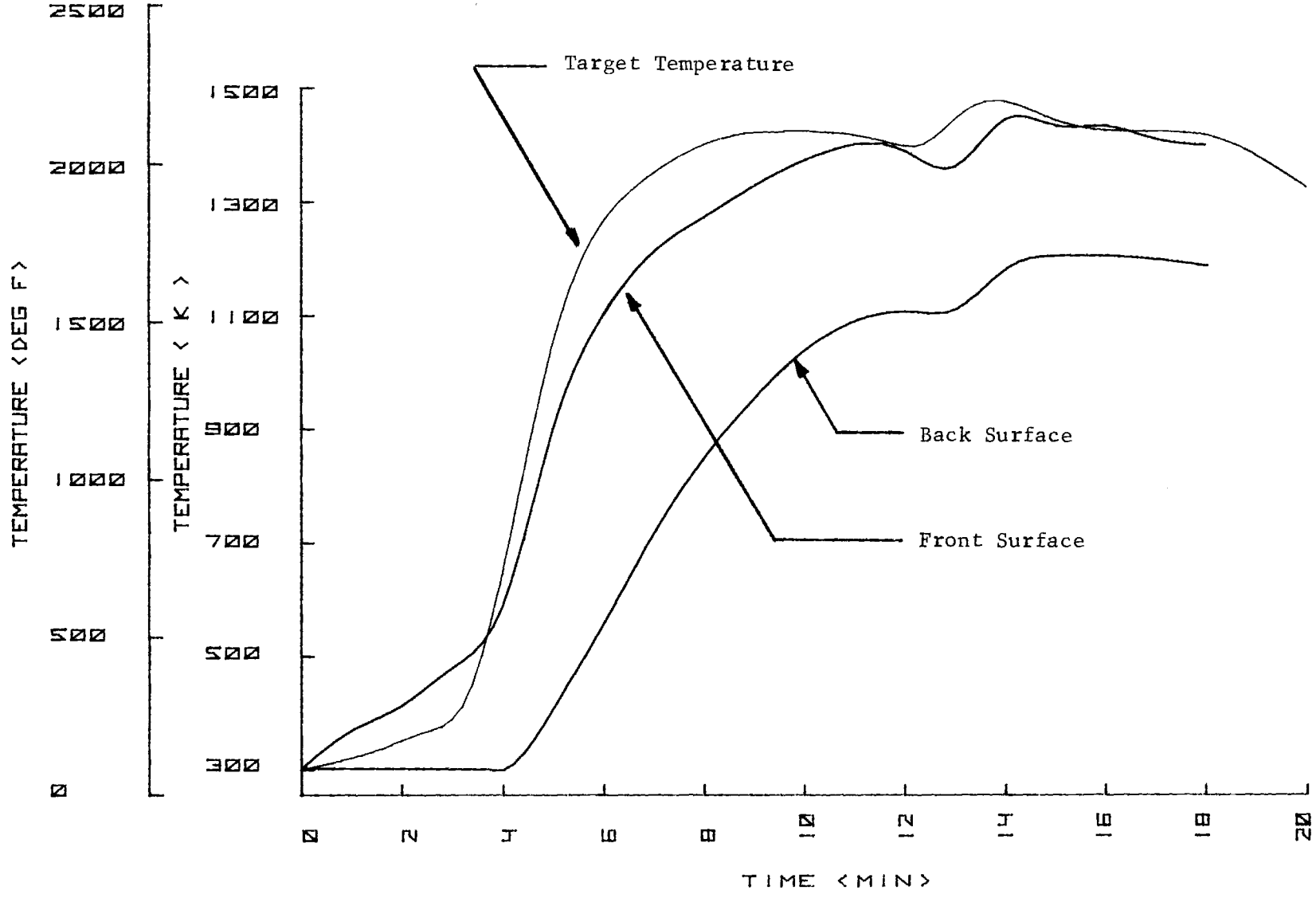

Figure 22. Typical Temperature versus Time Plot for LI-1500.

the smaller temperature gradient can both be attributed to the very high thermal conductivity of boron nitride.

The low density samples (Mullite HCF and LI-1500) both experienced high rates of front surface temperature rise, almost matching the target temperature profile. They reached the desired maximum temperature and had steep temperature gradients, on the order of 400° K (700° F) between the front and rear surfaces. The steep gradients and high rate of temperature rise can be attributed to their low thermal conductivity.

These results illustrate the influence of the thermal properties of materials on their temperature response to a reentry environment. Various materials responded differently even though heating conditions were reproduced as closely as possible; in fact different materials run on the same carrier disk showed different rates of temperature rise. There is no "representative dielectric window material" for thermal response calculations. Reentry temperature calculations must be run using appropriate thermal properties for each candidate material, to accurately predict the temperature which will be reached during a proposed reentry flight path.

Of the six specimen materials, only two showed any physical evidence of change after ten temperature cycles. Boron nitride (HD-0092) had a powdery deposit on both faces after removal from the carrier disk. The deposit on the front surface showed streaks, and was an estimated 0.5 mm thick; the deposit on the rear surface was smooth and somewhat thinner. Mullite HCF had lost some flakes of coating around the perimeter of the sample after removal from the carrier, and the remaining coating was loosely held to the porous substrate. Figure 23 shows microwave samples of each material after ten temperature cycles.

Electrical Data

The results of the microwave transmission measurements are presented in this section as dielectric constant and loss tangent of each sample versus temperature. The dielectric constant and loss tangent of McDonnell Mullite HCF vary with temperature as indicated in Figure 24. The dielectric constant increases by approximately 7 percent from room temperature to 1480° K (2200° F). The loss tangent increases from a room temperature value of 0.0003 to 0.068 at 1480° K (2200° F). This is a large change in loss tangent as compared to the

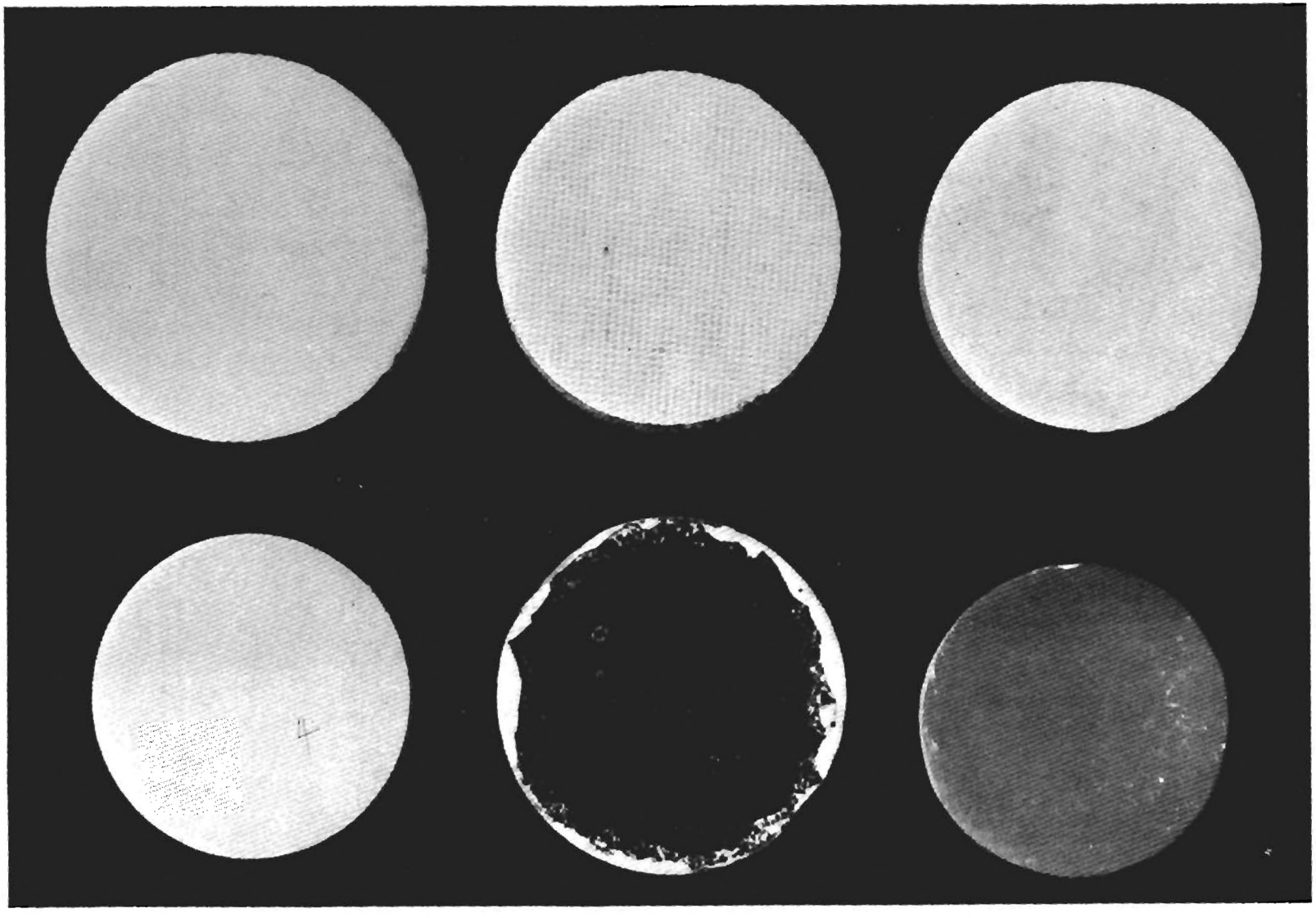

Figure 23. Sample Materials After Ten Temperature Cycles (from upper left: SCFS, AS-3DX, Markite 3DQ, Boron Nitride HD-0092, Mullite HCF, LI-1500).

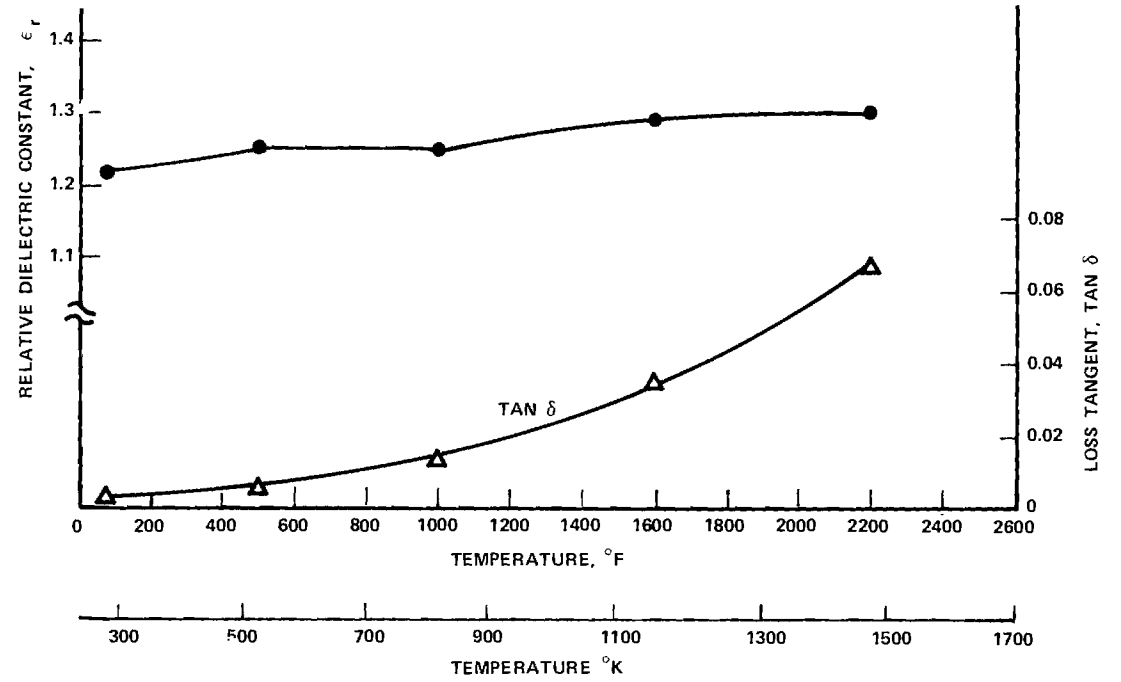

Figure 24. McDonnell Mullite Electrical Properties (ρ = 0.279 gm/cm^3).

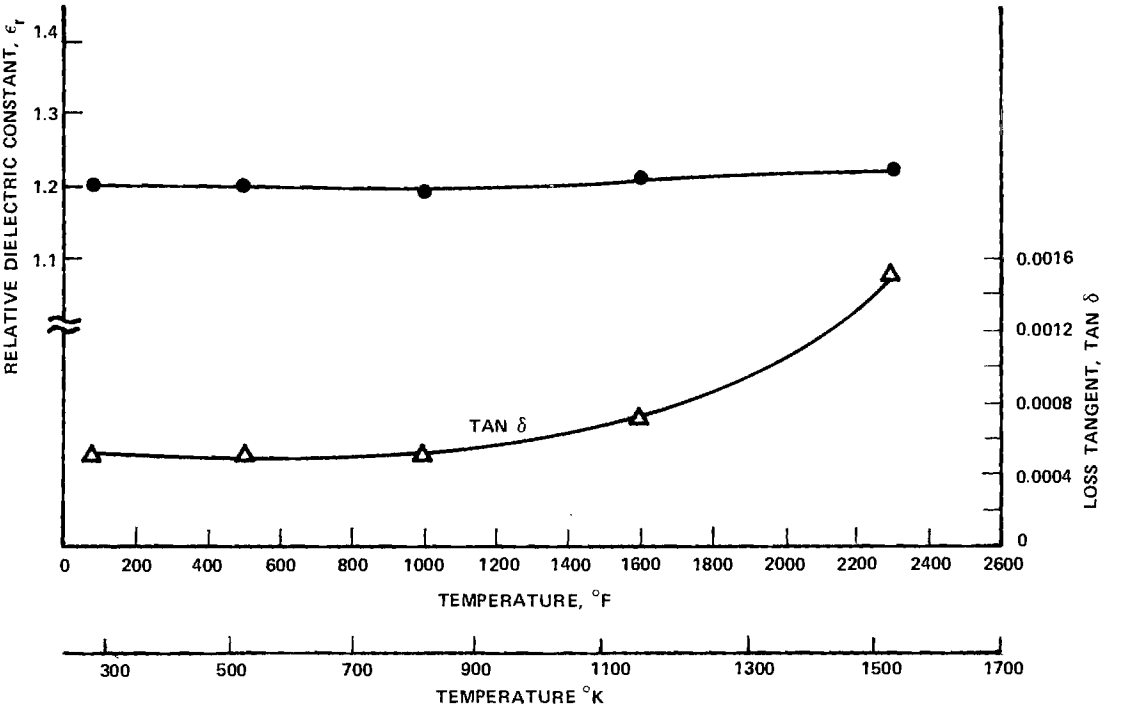

Figure 25. Lockheed LI-1500 Electrical Properties (ρ = 0.237 gm/cm^3).

other materials considered.

In Figure 25 are illustrated the electrical properties of Lockheed LI-1500. The dielectric constant increased by approximately 2 percent from room temperature to 1530° K (2300° F). The loss tangent increased from 0.0005 at 298° K (75° F) to 0.0015 at 1530° K (2300° F). Thus, the loss tangent increased very little over this temperature range.

The electrical properties of General Electric Markite are presented in Figure 26. The dielectric constant increases almost linearly from a 298° K (75° F) value of 3.17 to a value of 3.26 at 1255° K (1800° F). The loss tangent shows no increase with temperature to 1255° K (1800° F). Above 1255° K (1800° F), both the dielectric constant and loss tangent increase. The loss tangent shows a rapid increase.

The Philco-Ford AS-3DX material shows little change in either dielectric constant or loss tangent over the measured temperature range. These data are presented in Figure 27.

The electrical properties of the Georgia Tech slip-cast fused silica are illustrated in Figure 28. The dielectric constant increases only slightly up to 1366° K (2000° F). Above 1366° K (2000° F), the dielectric contant increases at a faster rate with temperature. The loss tangent indicates a linear increase from a value of 0.0005 at 298° K (75° F) to a value of 0.006 at 1644° K (2500° F).

In Figure 29 are presented the electrical properties of hot-pressed boron nitride. As indicated, the dielectric constant remains almost constant (ϵ_r = 3.93) to 810° K (1000° F) and from that point, the dielectric constant increases to a value of 4.05 at 1394° K (2050° F). The loss tangent remains very low from 298° K (75° F) to 588° K (600° F). It increases at a linear rate to 1394° K (2050° F). As previously stated, the boron nitride did ablate slightly during each measurement run.

All of the materials except McDonnell Mullite exhibit excellent low loss properties as functions of temperature. The McDonnell Mullite had a much higher loss tangent than the other materials tested, but this does not prohibit its use as a window material. This is especially true if other factors make it a better candidate for a particular application.

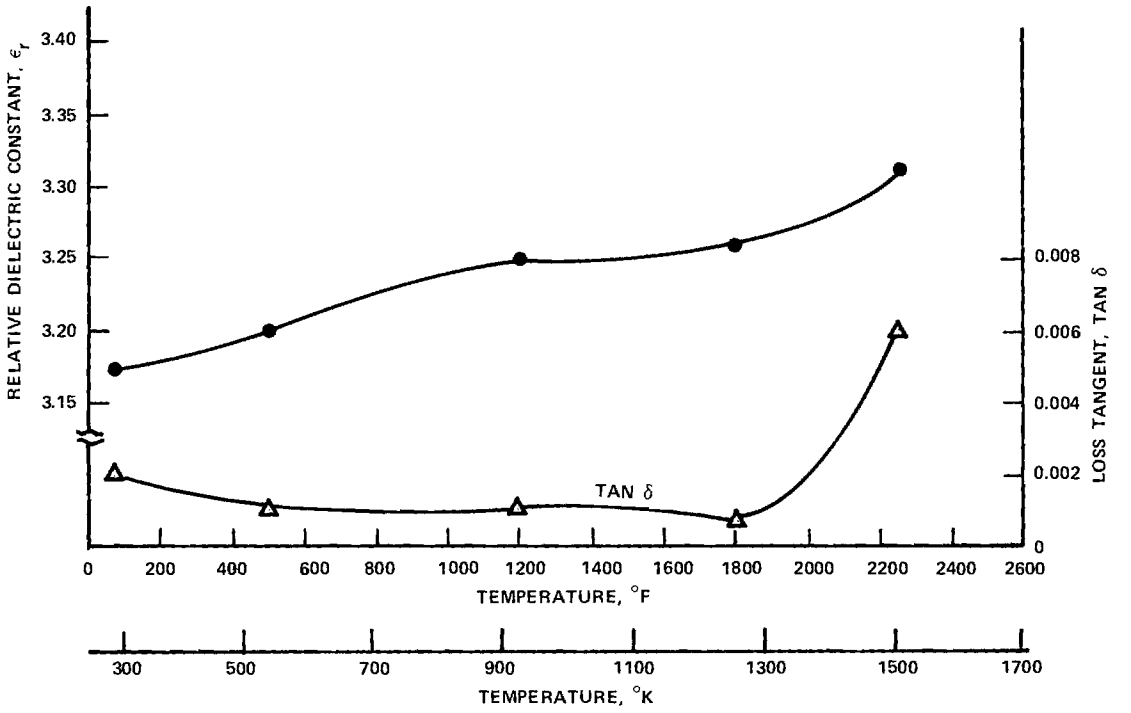

Figure 26. General Electric Markite Electrical Properties (ρ = 1.913 gm/cm^3).

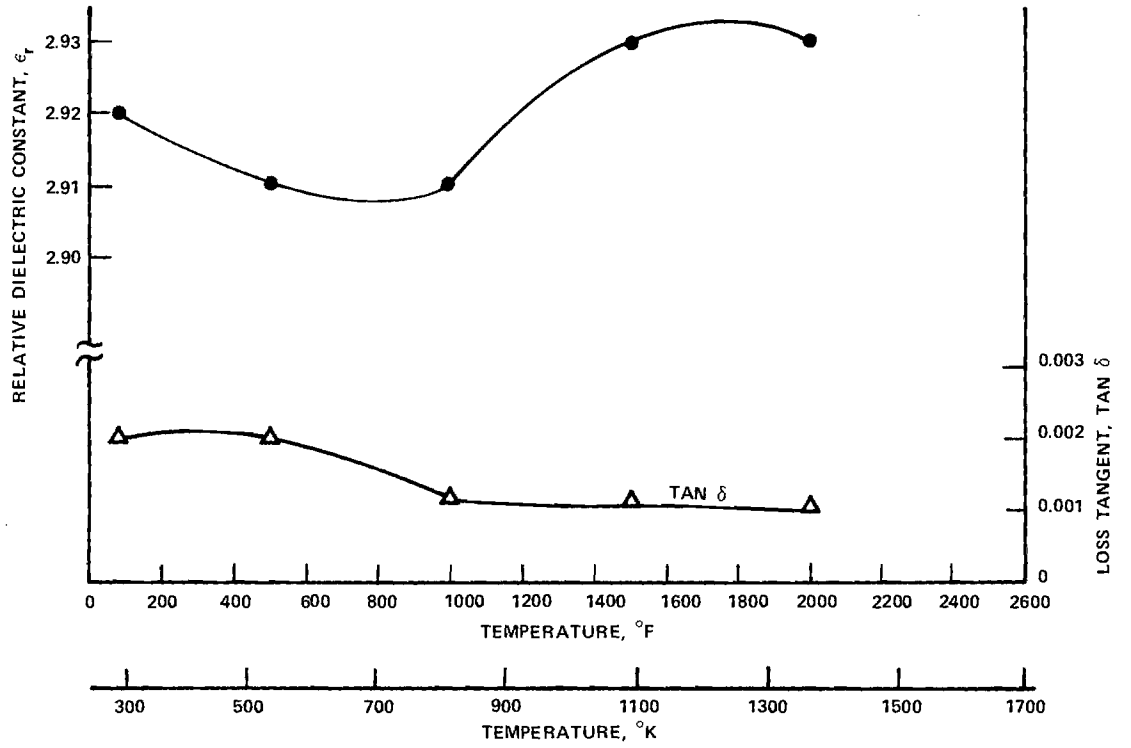

Figure 27. Philco-Ford AS-3DX Electrical Properties (ρ = 1.673 gm/cm^3).

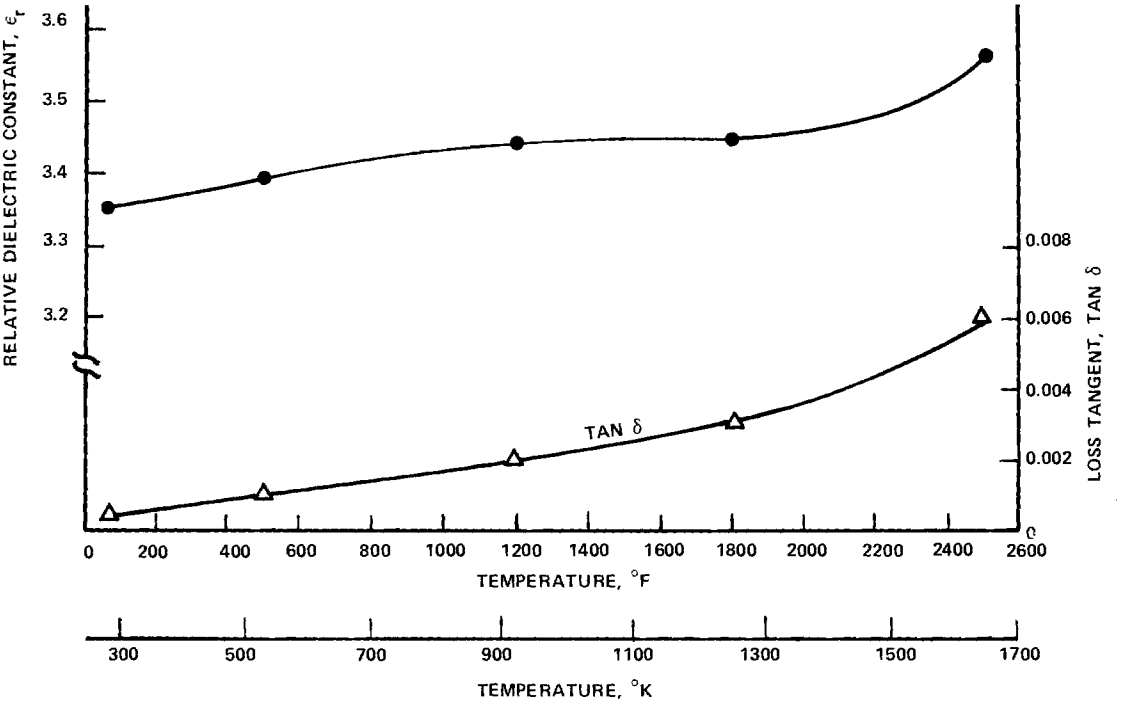

Figure 28. Georgia Slip-Cast Fused Silica Electrical Properties (ρ = 1.902 gm/cm^3).

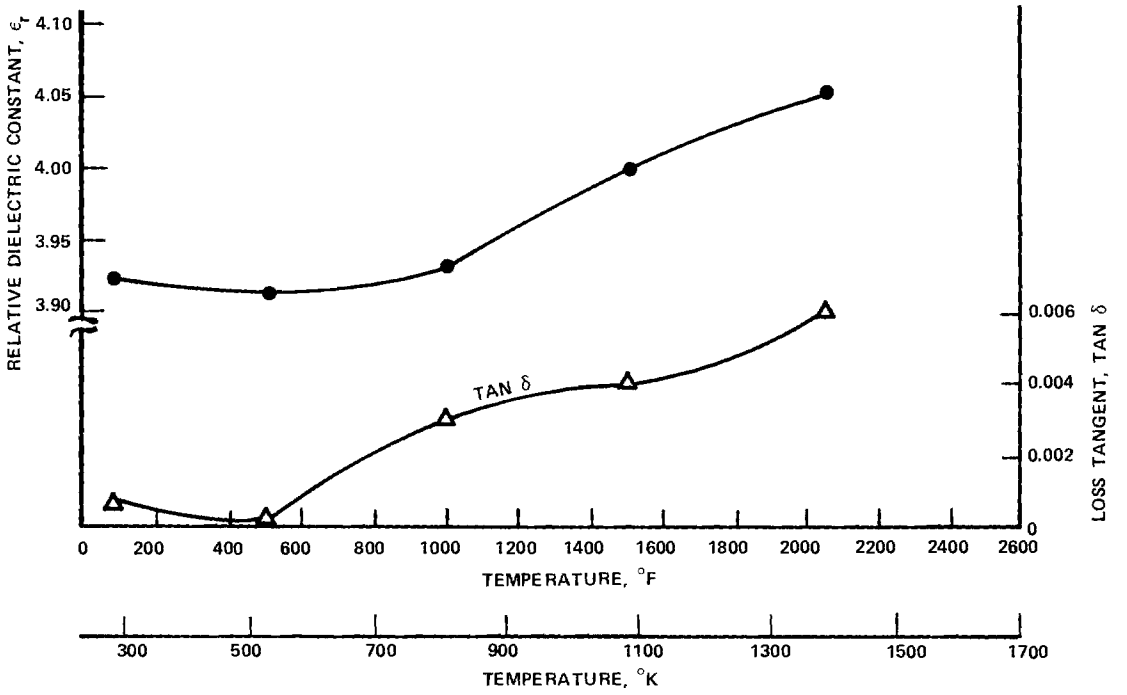

Figure 29. Hot Pressed Boron Nitride Electrical Properties (ρ = 1.976 gm/cm^3).

CONCLUSIONS

The following conclusions seem warranted from the results of this measurement program:

(1) A system was developed which permitted measurement of the microwave properties of candidate window materials during simulation of the Space Shuttle reentry thermal profile.

(2) None of the six materials tested showed significant deterioration in dielectric properties with repeated cycling through the specified reentry temperature profile, up to ten temperature cycles. AS-3DX showed small changes during the first two cycles.

(3) Four of the sample materials showed no visible deterioration in physical properties after ten reentry temperature cycles. Mullite HCF suffered loosening and chipping of its emittance control coating which might be serious in the presence of aerodynamic drag. Boron nitride lost thickness and developed powdery surface deposits, probably the result of oxidation; however, this does not appear to be a severe problem after ten temperature cycles.

(4) The dielectric constants and loss tangents of the sample materials as functions of temperature are within ranges that would not prohibit their use for Space Shuttle antenna windows. Mullite HCF had a higher loss tangent than the other candidates.

(5) A smaller program would be advisable to verify the acceptability of the final dielectric window design, once the material and reentry temperature profile have been firmly established.

APPENDIX

Thermal Analysis Computer Program

THERMAL ANALYSIS PROGRAM

```
00100      1*      C     HEAT CONDUCTION ANALYSIS, K AND CP FUNCTIONS OF TEMP
00101      2*            DIMENSION T(21),TLAST(21),ALPHA(21),DIST(21),RALFA(21),HEADNG(9),
00101      3*           1TIML(50),TS(50),TB(50)
00101      4*      C     REAL TIM,DELTIM,T,TLAST,DIST,ALPHA,RHO,CP,CA,CB,CC,THICK,DELX,R
00101      5*      C     REAL TIML,TS,TB,TIM1,TIM2,TS1,TS2,TB1,TB2,FSLOPE,BSLOPE,FINTCP
00101      6*      C     BINTCP,RALFA
00103      7*            REAL K,KA,KB,KC,KD
00103      8*      C     INTEGER I,J,J2,J3,L,LMAX,M,M2,NRUN,NRUNS
00103      9*      C     OUTPUT FORMATS
00104     10*          1 FORMAT(1H1)
00105     11*          2 FORMAT(/,6X,11HMATERIAL = ,9A6,/,9X,12HTHICKNESS = ,F5.3,5H INCH)
00106     12*          3 FORMAT (/,9X,26HHEAT CAPACITY COEFFICIENTS,/,12X,4HA = ,E10.3,/,
00106     13*           112X,4HB = ,E10.3,/,12X,4HC = ,E10.3,/,9X,33HTHERMAL CONDUCTIVITY C
00106     14*           20EFFICIENTS,/,12X,4HA = ,E10.3,/,12X,4HB = ,E10.3,/,12X,4HC = ,
00106     15*           3E10.3,/,12X,4HD = ,E10.3,/,9X,10HDENSITY = ,F6.2,7H LB/FT3,/,9X,
00106     16*           49HDELTIM = ,F6.3,4H SEC,/,9X,23HNUMBER OF TIME STEPS = ,I5,
00106     17*           5//,9X,31HTIME AND TEMPERATURE INPUT DATA,/,12X,10HTIME (MIN),6X,
00106     18*           617HSURF TEMP (DEG F),6X,17HBACK TEMP (DEG F))
00107     19*         14 FORMAT(13X,F7.1,14X,F6.1,17X,F6.1)
00110     20*         15 FORMAT (/,9X,15HELAPSED TIME = ,F8.3,4H SEC,/)
00111     21*         16 FORMAT (/,9X,7HSTATION,6X,13HDISTANCE (IN),6X,12HTEMP (DEG F),6X,
00111     22*           120HDIFFUSIVITY (FT2/HR),9X,5HRALFA)
00112     23*         17 FORMAT (12X,I2,11X,F5.3,14X,F5.0,15X,E9.3,14X,F6.4)
00112     24*      C     INPUT FORMATS
00113     25*         21 FORMAT(9A6,F10.3)
00114     26*         22 FORMAT(3E10.3)
00115     27*         23 FORMAT(4E10.3)
00116     28*         24 FORMAT(2F7.3)
00117     29*         25 FORMAT(3F10.0)
00120     30*         26 FORMAT(2I5)
00120     31*      C     READ INPUT DATA
00121     32*            READ(5,21) HEADNG,THICK
00130     33*            READ(5,22) CA,CB,CC
00135     34*            READ(5,23) KA,KB,KC,KD
00143     35*            READ(5,24) RHO,DELTIM
00143     36*      C     LMAX IS NO. OF TEMP INPUT CARDS,NRUNS IS NO. OF RUNS
00147     37*            READ(5,26) LMAX,NRUNS
00147     38*      C     CALCULATE DELX,R(UNITS FT AND HRS)
00153     39*            DELX = THICK/240.0
00154     40*            R = DELTIM/(3600.0*DELX**2)
00154     41*      C     M IS THE TOTAL NO. OF TIME STEPS IN THE CALCULATION AND
00154     42*      C     M2 IS THE NO. OF TIME STEPS BEFORE A PROFILE IS PRINTED
00155     43*            M = IFIX(1080.0/DELTIM)
00155     44*      C     M2=M/9 PRINTS PROFILE EACH 2 MIN, M2=M/18 PRINTS EACH MIN
00156     45*            M2 = M/9
00157     46*            NRUN = 0
00160     47*         30 READ(5,25) (TIML(L),TS(L),TB(L),L=1,LMAX)
00160     48*      C     WRITE INPUT DATA
00170     49*            WRITE(6,11)
00172     50*            WRITE(6,12) HEADNG,THICK
00201     51*            WRITE(6,13) CA,CB,CC,KA,KB,KC,KD,RHO,DELTIM,M
00215     52*            DO 31 L=1,LMAX
00220     53*            WRITE(6,14) TIML(L),TS(L),TB(L)
00225     54*         31 TIML(L) = TIML(L)*60.0
00225     55*      C     SET INITIAL VALUES OF VARIABLES
00227     56*            DO 32 I=1,21
00232     57*            DIST(I)=(DELX*FLOAT(I)-DELX)*12.0
```

```
00233     58*          32 TLAST(I) = 540.0
00235     59*             TIM = DELTIM
00236     60*             J2 = 1
00237     61*             J3 = 0
00240     62*             L=0
00241     63*             TIM1=0.0
00242     64*             TIM2=0.0
00243     65*             TS2=80.0
00244     66*             TB2=80.0
00244     67*       C     START TIME LOOP
00245     68*             DO 50 J=1,M
00245     69*       C     CALCULATE FRONT AND BACK SURFACE TEMPS, WHEN TIM HAS PASSED THE
00245     70*       C     END OF PRESENT INTERPOLATION LINE, CALCULATE NEW LINE
00250     71*             IF(TIM-TIM2)35,35,34
00250     72*       C     CALCULATE NEW INTERPOLATION LINE
00253     73*          34 TS1=TS2
00254     74*             TB1=TB2
00255     75*             TIM1=TIM2
00255     76*       C     READ A NEW DATA POINT
00256     77*             L=L+1
00257     78*             TIM2=TIML(L)
00260     79*             TS2=TS(L)
00261     80*             TB2=TB(L)
00262     81*             FSLOPE=(TS2-TS1)/(TIM2-TIM1)
00263     82*             BSLOPE=(TB2-TB1)/(TIM2-TIM1)
00264     83*             FINTCP=TS1-FSLOPE*TIM1+460.0
00265     84*             BINTCP=TB1-BSLOPE*TIM1+460.0
00265     85*       C     FIND SURFACE TEMP FROM LINE
00266     86*          35 T(21)=FSLOPE*TIM+FINTCP
00267     87*             T(1)=BSLOPE*TIM+BINTCP
00267     88*       C     CALCULATE INTERIOR STATION TEMPS
00270     89*          37 DO 40 I=2,20
00273     90*             K=KA+(KB/TLAST(I))+KC*TLAST(I)+KD*(TLAST(I)**3)
00274     91*             CP=CA+CB*TLAST(I)+CC/((TLAST(I))**2)
00275     92*             ALPHA(I)=K/(CP*RHO)
00276     93*             RALFA(I)=R*ALPHA(I)
00277     94*          40 T(I)=TLAST(I)+ALPHA(I)*R*(TLAST(I+1)+TLAST(I-1)-2*TLAST(I))
00277     95*       C     DECIDE WHETHER TO PRINT, WHEN J2=M2, PRINT
00301     96*             IF(J2-M2) 42,43,43
00304     97*          42 J2=J2+1
00305     98*             GO TO 48
00305     99*       C     DECIDE WHETHER TO TURN PAGE, WHEN J3=0, TURN PAGE
00306    100*          43 IF(J3-1) 44,45,45
00311    101*          44 WRITE(6,11)
00313    102*             J3=1
00314    103*             GO TO 46
00315    104*          45 J3=0
00316    105*          46 WRITE(6,15) TIM
00321    106*             WRITE(6,16)
00323    107*             DO 47 I=1,21
00326    108*             TLAST(I)=T(I)
00327    109*             T(I)=T(I)-460.0
00330    110*          47 WRITE(6,17)I,DIST(I),T(I),ALPHA(I),RALFA(I)
00330    111*       C     TO PUNCH FINAL PROFILES ADD WRITE AND FORMAT 27 CARDS HERE
00340    112*             J2=1
00341    113*             GO TO 50
00341    114*       C     SET UP FOR NEXT TIME LOOP
00342    115*          48 DO 49 I=1,21
00345    116*          49 TLAST(I)=T(I)
00347    117*          50 TIM=TIM+DELTIM
00351    118*             NRUN = NRUN+1
00351    119*       C     WHEN NRUN=NRUNS, YOU ARE FINISHED
00352    120*             IF(NRUN-NRUNS) 30,60,60
00355    121*          60 WRITE(6,11)
00357    122*             STOP
00357    123*       C     DATA CARDS FOLLOW XQT CARD
00360    124*             END
```

END OF COMPILATION: NO DIAGNOSTICS.

REFERENCES

1. Bassett, H. L. and Bomar, S. H., Jr.: Dielectric Constant and Loss Tangent Measurement of High-Temperature Electromagnetic Window Materials. Proceedings of the Tenth Symposium on Electromagnetic Windows held at the Georgia Institute of Technology, July 29-31, 1970. pp. 187-191.

2. Bassett, H. L.; Bomar, S. H., Jr.; Huddleston, G. K.; and Merritt, A. C.: High-Temperature Complex Permittivity Measurements on Antenna Window Materials. Proceedings of the Eleventh Symposium on Electromagnetic Windows held at Georgia Institute of Technology, August 2-4, 1972. pp. 139-143.

3. Westphal, W. B.: Dielectric Constant and Loss Measurements on High Temperature Materials. MIT Laboratory for Insulation Research Technical Report 182, October 1963.

4. Westphal, W. B.; and Sils, A.: Dielectric Constant and Loss Data. Technical Report AFML-TR-72-39, Air Force Materials Laboratory, April 1972.

5. Kellerher, K. S.; and Bowie, D. M.: Rapid Measurement of Dielectric Constant and Loss Tangent. IEEE Transactions on Microwave Theory and Techniques, MIT-4, July 1958, p. 137.

6. Gilreath, M. C.; and Castellow, S. L., Jr.: High-Temperature Dielectric Properties of Several Candidate Space Shuttle Thermal Protection System and Antenna Window Materials. Proceedings of the Eleventh Symposium Electromagnetic Windows held at Georgia Institute of Technology, August 2-4, 1972. pp. 139-143.

7. Roberts, S.; and Von Hippel, J.: Journal of Applied Physics, Vol. 17, 1946, p. 610.

8. Dakin, T. W.; and Works, C. N.: Microwave Dielectric Measurements. Journal of Applied Physics, Vol. 18, September 1947, pp. 789-796.

9. Redheffer, R. M.: The Measurement of Dielectric Constant: in Technique of Microwave Measurements. Ed. by C. G. Montgomery, Mc-Graw-Hill, (New York), 1947.

10. Jakob, N.: Heat Transfer. Vol. I John Wiley and Sons (New York), 1949, p. 38.

11. O'Brien, G. G.; Hyman, M. A.; and Kaplan, S.: A Study of the Numerical Solution of Partial Differential Equations. J. Math. Phys., Vol. 29, 1951, pp. 223-251.

12. Lewis, G. N.; and Randall, N.: Thermodynamics, 2nd Edition. Revised by Pitzer, K. S.; and Brewer, L., McGraw-Hill Book Co. (New York), 1961, 723 p.

13. Jakob, M.: Heat Transfer. Vol. I. John Wiley and Sons (New York), 1949, pp. 102-107.